

Chapter 1

Introduction

1.1 Introduction

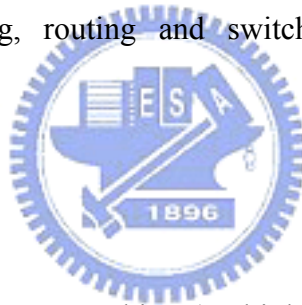
As the Internet and modern communications becomes increasingly prevalent across the globe, fiber optics as the defects infrastructure that supports the information revolution is racing to keep up. The demand for Internet services is driving the growth of data traffic worldwide. Software developers and users are constantly adopting applications that devour more and more bandwidth in order to speed delivery of information. As multiple forms of traffic place increasingly heavy burdens on fiber networks, carriers are looking for innovative ways to push more data through existing fiber. Dense wavelength division multiplexing (DWDM) technology is an effective way to increase the transmission bandwidth of optical communication systems. A number of different designs of DEMUXs have been implemented in the past, using gratings [1], thin film structures [2], fiber Bragg gratings [3], and arrayed waveguide gratings [4], etc.

Conceptually, the WDM scheme is the same as FDM used in microwave radio and satellite systems. WDM technology, by which multiple optical channels can be transmitted at different wavelengths through a single optical fiber simultaneously and independently, is a cost-effective method of making full use of the low-loss characteristics of optical fibers over a wide-wavelength region [5]-[7]. Data networks with DWDM have experimentally demonstrated terabit-per-second transmission [8].

1.2 Introduction of DWDM

DWDM technologies had been employed for backbone network and long-haul services in the past. An entirely new area has now opened in the local area network right down to consumer owing to the bandwidth demand. DWDM techniques can provide the needed capacity and offer the reconfiguration flexibility for local area network[9].

The use of DWDM gives possibilities to send at several channels on various wavelengths at once in a single fiber. The discrete wavelengths form an orthogonal set of carriers, which gives possibilities to perform network and system oriented functions such as separating, routing and switching the wavelengths without interfering with another.



1.2.1 DWDM Structure

A DWDM must be able to combine (multiplex) a number of closely spaced wavelengths on a single fiber and also to separate (demultiplex) each wavelength from a single fiber into a number of fibers, each containing only one wavelength. Multiplexing and demultiplexing must be done with low loss and with a high degree of isolation between wavelengths to minimize channel crosstalk[10].

Mux and Demux both employ narrowband filters, cascaded and combined in several ways to achieve the desired result. Several techniques that have been used to perform such a filtering function include thin-film filters, fiber Bragg grating filter, liquid crystal filters, and Mach-Zehnder and waveguide-grating routers. Mux/Demux device are available now to handle the 100 GHz(0.792 nm) channel spacing.

1.2.2 Multiplexers and Demultiplexers

The output of each laser transmitter in a WDM system is set to one of the allowed channel frequencies. These beams must then be multiplexed – superimposed or combined – and inserted into the first fiber cable span. The device used is called a multiplexer (also called a mux, optical mux, or OM). A similar device is used to extract the multiplexed channels at the receiver end of each link. It is called a demultiplexer (or demux, optical demux, or OD). Unlike the situation in TDM systems, where both these operations occur in the time domain and much attention must be paid maintaining accurate clocks and to retrieving timing clues from incoming signals, multiplexing and demultiplexing in WDM systems are strictly a matter of dealing individually with a signal’s spectral components. The characteristics of these spectral components are always known beforehand.

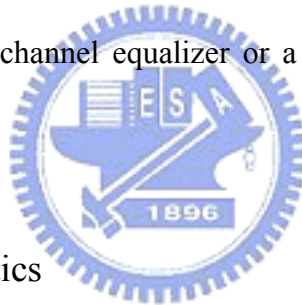
Multiplexing and demultiplexing functions both employ narrowband filters, cascaded and combined in other ways to achieve the desired result. Particular techniques that have been used to perform such filtering include thin-film filters, fiber Bragg or bulk optic gratings, tapered fibers, liquid crystal filters, and integrated optics (phased array waveguides, AWG, or phasar).

Many mux/demux devices are available today to handle the 100 GHz (0.792nm) channel spacing that is common in WDM networks, and to accommodate the more demanding 50 GHz spacing – or even higher channel densities – that are appearing. Most recent models have been based on thin-film filters, with arrayed waveguides and fiber Bragg grating models close behind, but this technology distribution will shift as more stringent requirements of narrowly spaced DWDM systems come to bear.

1.3 The Characteristics and various technologies of optical equalizers

In a wavelength-division-multiplexing (WDM) optical network, it is important to maintain equal signal power levels over the WDM spectrum in order to avoid signal-to-noise ratio degradation. Power nonuniformities occur due to the nonflat spectral responses of components in the network. For example the nonflat gain spectrum of an erbium-doped fiber amplifier (EDFA) leads to a power imbalance of the WDM channels.

To restore the power balance of the WDM channels one can correct every channel individually using a channel equalizer or a de-mux/mux combination with variable optical attenuators.



1.3.1 Device Characteristics

(1) Ripple level (SNR: Signal to Noise Ratio)

Fluctuation, after the optical equalizer, the Peak to Peak value of optical power, it's a index for the optical equalizers. Signal-to-noise ratio is ratio of signal power against noise power for the receiver.. SNR is usually described in decibels, or "dB", for short; the bigger the number, the better looking the picture.

(2) Wavelength range

The trend nowadays is to increase the gain bandwidth of EDFAs to include not only conventional-band *C*-band wavelengths (1530-1560 nm), but also long-band *L*-band wavelengths (1570-1620 nm) in order to accommodate the bandwidth-hungry Internet-based applications of the near future. We hope to get the flat gain spectrum of

an erbium-doped fiber amplifier, there are the applicable range for variable optical attenuators.

(3) Insertion loss (IL)

IL is loss of optical energy resulting from the insertion of a component or device into the optical path.

The insertion loss and bandwidth both parameters should be referenced to the same point. Another parameter related to the insertion loss is uniformity or flatness, how does the insertion loss change across channels.

(4) Attenuation ratio

Attenuation ratio is the diminution ratio of average optical power. Attenuation results from absorption, scattering, and other radiation losses. Attenuation is generally expressed in dB without a negative sign.

These optical equalizers often are attenuator. By lessening the power to flat signal power levels over the WDM spectrum. Attenuation ration have the deciBel (dB) and percentage.

(5) Polarization dependence loss (PDL)

PDL is the difference in dB between the maximum and minimum values of loss (attenuation) due to the variation of the polarization states of light propagating through a device.

Many of the parameters such as bandwidth, center wavelength, and insertion loss are dependent on the state of polarization. When the polarization varies, the shape of the DEMUX function will change.

1.3.2 Variety of Technologies For optical equalizers

(1) Mach-Zehnder interferometer[11-14]

A schematic drawing of a two-stage RC device. In this device the delay lines, which are all of equal length, set the free spectral range (FSR) of the response. A one-stage device is a simple asymmetrical MZI and its response can be described with one harmonic. With more stages, the spectral response is a Fourier-series-type function with the highest harmonic having a periodicity of FSR/N , where N equals the number of stages. The ability to flatten an arbitrary gain spectrum increases with the number of stages and requires full tunability of all the coupling and delay line sections.

(2) Dynamically gain-flattened erbium-doped fiber amplifiers (DGF-EDFAs)[15]

DGF-EDFA comprising a well-designed static gain-flattening filter (GFF) and a voltage-controllable fiber-based gain tilt controller (GTC) and a digital signal processor (DSP). The DSP calculates the amplitude and the wavelength shift, and the driver circuit applies an accurate biasing voltage to the dynamic GTC, working together with the static GFF to achieve the required flattened gain profiles. The tuning range is determined by the required EDFA gain slope change.

(3) Acousto-optic tunable filters(AOTF)[16]

The AOTF is based on mode conversion from the core mode to the dissipating cladding modes by periodic microbends formed by acoustic waves. The acoustic wave is generated by a piezoelectric transducer and launched to a single-mode fiber (SMF) by using a silica glass horn. Each AOTF was operated with three RF signals at different frequencies. Each RF signal produces an individual notch in the transmission spectrum of the AOTF. By tuning the frequencies and voltages of the six RF signals,

the overall filter profile can be controlled to match a very complex shape needed for gain flattening of an EDFA.

In the experiment, the computer controlled only the voltages of the radio-frequency (RF) signals, and the frequencies of the RF signals were fixed to specific preset values for simplicity. It turned out that the voltage feedback control was sufficient for the EDFA to respond to various operating conditions successfully as described in the following. Better feedback algorithm for system implementation is under study.

(4) Long-period fiber-grating-based gain equalizers[17-19]

LPGs are demanding and interesting because of low insertion loss and back reflection. When we manufacture a long-period change of dielectric constant, transmittance will be control. There are some kinds of methods to make up. One usually fabricates LPGs by use of UV radiation to induce a periodic index change of the fiber core. Second, they used periodic microbends induced by electric arcs and mechanically pressed a plate with periodic grooves against a short and long length of fiber. This filter, which is very simple and inexpensive

(5) Etalon-Type Gain-Flattening Filter[20]

The Fabry – Perot etalon filter named after its inventors can be considered an archetype of the optical resonator and it is a one-dimensional resonator. It uses interference phenomena of multiple reflections between mirrors paralleled in medium. The etalon-type GFF consists of several etalon filters with different amplitudes and phases to compensate asymmetric EDFA gain wavelength characteristics for flattening gain shapes.

In the design process, the number of etalon filters composing GFF and the thickness and phase of each etalon filter, in other words, reflectance and thickness of etalon filters and incident angle, are acquired.

By using this method we can design an etalon-type gain-flattening filter with superior characteristics for flattening EDFA gain – wavelength characteristics.

(6) Liquid-Crystal Optical Harmonic Equalizer[21-25]

Liquid-Crystal Optical Harmonic Equalizer has multiple stages of harmonic elements. Each stage includes a liquid-crystal harmonic filter to adjust the wavelength shift and a liquid-crystal attenuator to adjust the amplitude of harmonic waveform. The optical spectrum analyzer obtains power profiles at the input/output ports of OHE and the output of second EDFA. The digital signal processor (DSP) compares the data with the desired gain profile, which can be accessed through the user interface, and calculate the required transfer function to flatten the power profile. The DSP then calculate the amplitude and wavelength shift for each harmonic element by expanding the required transfer function in a Fourier series. The driver circuit applies accurate biasing voltages on the liquid-crystal modulators to achieve the required harmonic shapes.

(7) Arrayed Waveguide Grating (AWG) filter[26-27]

The equalizer is made in silica waveguides on a silicon substrate. The waveguide core index is $\sim 0.65\%$ higher than the cladding. The design is a Mach–Zehnder interferometer with a grating-lens-grating cascade in one arm. We will call this arm the filtered arm, and the other, the nonfiltered arm. The interferometer employs $\sim 50/50$ evanescent couplers and is in the cross-state (one fiber is glued to an upper input and the other to a lower) to reduce the wavelength dependence and fabrication

uncertainty of the couplers. The gratings have 60 waveguides each, and there are 61 lens inlets per grating free-spectral range, the central 44 of which on each side are connected to each other by equal-length waveguides. Thus the optical spectrum is slightly oversampled, allowing the device to perfectly reconstruct the input spectrum over the band of interest, if so desired. Each lens waveguide, as well as the nonfiltered arm, contains a thermo-optic phase shifter, consisting of a chrome heater (3.8 mm 38 m) over the waveguide. The phase shifters are spaced by 100 m.

From above statement, we know there are many kinds of skill to modulate the laser source. They have difference advantages and defects, now we can't determine which one will be best one. **Table 1-1** summarizes the data of Variety of Technologies For optical equalizers.



Table 1-1 The data of the Variety of Technologies For optical equalizers

	Ripple Level (dB)	Wavelength(nm)	Insertion loss(dB)	Attenuation ration(dB)	PDL	Feedback control
Mach-Zehnder interferometer	0.5 ~ 0.9	69nm (1540 ~ 1609)	9dB	25dB	0.5dB	possible
Dynamically gain-flattened erbium-doped fiber amplifiers	6dB (0.8dB)	1528 ~1602	9dB	>14dB		can
Acousto-optic tunable filters	0.6dB	Over 30nm (1529 ~1559)				can
Long-period fiber-grating-based gain equalizers	<1dB	33nm (1524.3~1558.)			0.3dB	cant
Etalon-Type Gain-Flattening Filter	0.32dB	35nm (1530 ~ 1565)	0.8dB		0.05dB	cant
Liquid-Crystal Optical Harmonic Equalizer	0.6dB	1528 ~ 1576	4.5dB	>10dB	0.15dB	can
Arrayed Waveguide Grating(AWG) filter	~0.5dB	1530 ~ 1562.7	~2.8dB	>14dB	0.24dB	cant

1.4 Objectives

First, We studied many kinds of tuning mechanisms of Extended-cavity diode lasers(ECDL).Wavelength tunable, single-frequency semiconductor lasers with the Littrow or Littman/Metcalf configurations are valuable components for optical communications, high-resolution measurements of displacement, spectroscopy and so on[28-30].In particular, liquid crystal devices have been employed successfully as electronically tunable spectral filters for wavelength selection in these lasers and related WDM systems[31-36].

On the other hand, liquid crystal devices have long been developed for WDM. Previously, a six-port DEMUX using a liquid crystal etalon was fabricated [37].

Liquid crystal polarization rotators and Wollaston beam deflectors were employed in a symmetric grating-based system to construct 1×2 switches that can switch independently 8 wavelength channels 4 nm apart [38]. 100-GHz-resolution dynamic channel management was accomplished by using in-line liquid crystal spatial light modulator (LC-SLM) and a grating together in the collimated beam of a 4-f relay optic system between input and output single-mode fibers. For DWDM applications in metropolitan area networks and local area networks, multimode DEMUXs are attractive. A compact athermalized low-loss 8-channel 200-GHz grating-based multimode DEMUX with low IL and low thermal effect has recently been reported [39].

In this work, we present a new liquid-crystal-based multimode demultiplexer or LC-multi-DEMUX. It differs from the previous design in three aspects:

- (1) The LC-SLM is placed at the focal plane of the folded telescopic grating system;
- (2) Every other pixel of the LC-SLM was matched to one multi-mode fiber channel;
- (3) We can control pixels of the LC-SLM by feedback-control in order to equalizer the power of different channels.

This design is derived from our previously work on electrically controlled tunable external cavity semiconductor lasers and filters using LC-SLM technology [40-42]. A 16-channel 100-GHz DEMUX with channel switching or routing function as well as power equalization is demonstrated.

1.5 Organization of the thesis



In this thesis, we have developed a liquid-crystal-based 16-channel tunable optical DEMUX and Optical Demultiplexer feedback control Pixel Equalizer. This thesis consists of five chapters. Chapter 1 is basis introduction. Chapter 2, we describe the basic concept design of tunable DEMUX and ECDL. In chapter 3 we describe the DEMUX experimental system setup, characteristics of the LC-SLM, and experimental results of tunable optical demultiplexer. Chapter 4, we demonstrated a new designed Optical Demultiplexer feedback control Pixel Equalizer. Finally chapter 5 gives the conclusions.

Chapter 2

Basic Principles

2.1 Principles of wavelength demultiplexing

2.1.1 Diffraction grating operation principles

A diffraction grating consists of a large number of periodic spaced grooves on a substrate. The gratings are mainly divided into four categories: reflection amplitude and phase gratings (Fig. 2.1(a)); transmission amplitude and phase gratings (Fig. 2.1(b)). Take reflection amplitude grating for example, the light will reflect periodically by the grooves.

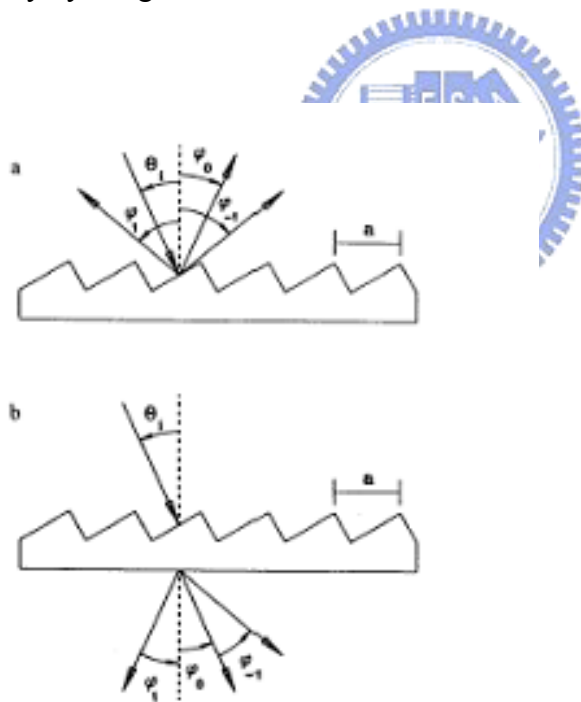


Fig. 2-1 Types of plane diffraction gratings (a) Reflection grating. (b)Transmission grating

Each diffracted wavelength from the grooves interferes each other, and then the constructive interference of the diffracted wavelength components from each groove occurs at unique set of discrete directions called the diffraction orders of the grating.

The constructive interference occurs when satisfying the grating equation below:

$$a(\sin \theta_i + \sin \theta_m) = m\lambda \quad (2.1)$$

where a is the groove spacing (pitch), θ_i is the incident angle, θ_m is the diffracted angle of the m 'th order, and m is the diffraction order. The diffraction light is dispersed according to its wavelength components, with different wavelengths diffracted at different angles. Differentiating the grating equation gives the angular dispersion D , which describes how much the diffraction angle changes as the wavelength varies:

$$D = \frac{d\theta_m}{d\lambda} = \frac{m}{a \cos \theta_m} = \frac{(\sin \theta_i + \sin \theta_m)}{\lambda \cos \theta_m} \quad (2.2)$$

According to the principles of multi-slits diffraction, the diffracted angle has undistinguishable distribution for monochromatic light.

$$\Delta \theta_m = \frac{\lambda}{Na \cos \theta_m} \quad (2.3)$$

where N is the total numbers of diffracted grooves. In other words, Na is the total diffracted width of grating. Note the $\Delta \theta_m$ is inversely proportional to Na . Obeying

the definition of Rayleigh's criterion and substituting $\Delta \theta_m$ into the equation (2.2) gives the wavelength resolution:

$$(\Delta \lambda)_{\min} = \frac{\lambda}{mN} \quad (2.4)$$

This is also called limit of resolution of grating. The *resolving power* R is defined in general by

$$R \equiv \frac{\lambda}{(\Delta \lambda)_{\min}} = mN \quad (2.5)$$

Diffraction gratings are usually used in first order, i.e. $m=1$, in tunable optical demultiplexer experiments.

2.1.2 Grating common mountings

There are two types for grating mounting [43]: one is Littrow mounting (Fig. 2.2), the other is the Littman mounting (grazing incident) (Fig. 2.3). In Littrow-mounting figure, the angles of incidence and diffraction are almost equal: $\theta_i = \theta_m$. The grating equation becomes

$$(2.1) \rightarrow \lambda = 2a \sin \theta_i \quad (2.6)$$

and angular dispersion also becomes

$$(2.2) \rightarrow D_{Littrow} = \frac{d\theta_i}{d\lambda} = \frac{2 \tan \theta_i}{\lambda} \quad (2.7)$$

A typical angle of incidence for the Littrow configuration is $\theta_i \sim 50^\circ$.

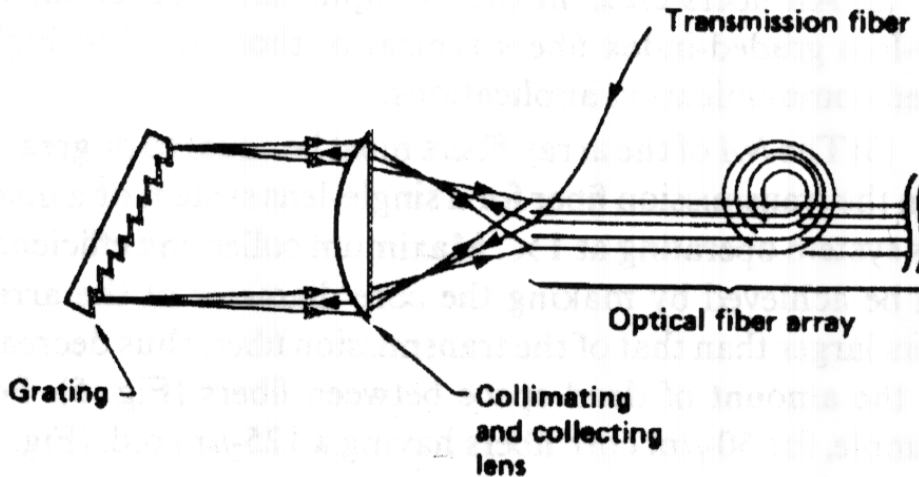


Fig. 2-2 Littrow mounting configuration

The advantage of Littrow mounting is to use a single lens. In the other hand, the disadvantage of this design is the required vicinity of the transmission fiber (input fiber) to fiber array (output fibers). If the transmission fiber is attached to the fiber array, moving fiber array also moves the transmission fiber and directly influences the image of transmission fiber on to output fiber. The alignment is very difficult.

In the grazing-incidence configuration (Figure 2.3), the incident angle is approximately equal to 90° , for example, $\theta_i \sim 85^\circ$ typically.

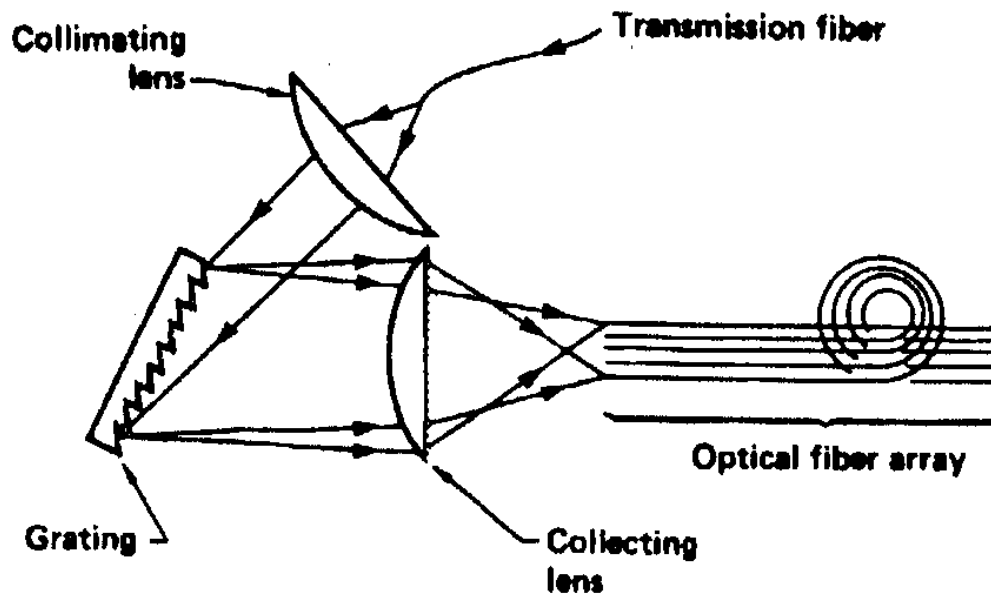


Fig. 2-3 Littman (grazing-incident) mounting configuration

The advantage of grazing-incident mounting is to avoid the above problem and to have ability to reject stray light. In the other hand, the disadvantage of this design is to use dual-lens at expense of some loss in efficiency.

2.1.3 Grating efficiency

The phase grating provides greater diffraction efficiency more than amplitude grating generally. In addition, blazing design used to maximize the efficiency. Blazing refers to an enhancement in efficiency that is obtained at a particular wavelength when the grooves on the grating surface have a triangular shape. The blaze wavelength λ_B at which this reinforcement occurs is called the “blaze angle” (angle of groove’s normal and optical grating’s normal). The terminology derives from the observation that a grating will light up or “blaze” when viewed at the correct angle. The grating efficiency is key parameter to determine insertion loss of grating based

devices. The grating efficiency against wavelength is required to be flat, wide, and high.

2.1.4 Theory of LC-based tunable optical demultiplexers/filters

Our tunable optical demultiplexer configuration is based on the spatial dispersion of grating and transmitted wavelength selected by LC-SLM, which will be described in next section. According to Eq. (2.1), the first differentiation is as below:

$$d\lambda = a \cos \theta_m d\theta_m \quad (2.8)$$

An AR-coating convex lens is applied to focus the dispersed wavelengths onto the focal plane (see Figure 3.1). Then, at the focal plane, we obtained different displacement with changing the first-diffracted angle:

$$dx \approx f d\theta_m \quad (2.9)$$

The above equation can divide by equation (2.9), and then the wavelength difference $d\lambda$ is transformed into the space coordinate difference dx in following equation below:

$$dx = \frac{f}{a \cos \theta_m} d\lambda \quad (2.10)$$

2.1.5 Coupling into fiber issue

To achieve efficient coupling into fiber, two conditions must be met [44]. First, the focused spot diameter from focused beam should be less than or equal to the mode field diameter (MFD) of the single-mode fiber (SMF) or core diameter of multi-mode fiber (MMF). Secondly, the numerical aperture (NA) of the focused beam should not exceed the NA of the fiber.

Given a lens with a focal length f , and focused spot size w , the two conditions will be:

$$w \leq a$$

$$NA_{ray} = \frac{D}{2f} \leq NA_{fiber} \quad (2.11)$$

where D is collimated beam diameter and a is the core diameter of MMF

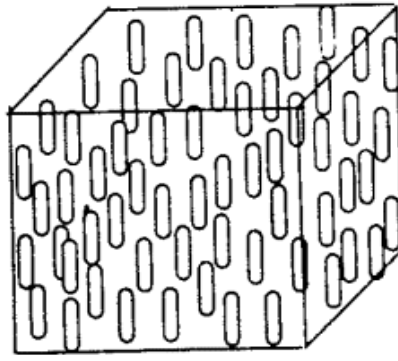
or the MFD of SMF. Note w will be $\frac{4}{\pi} \lambda \frac{f}{D}$ for Gaussian beam. If

possible, try to select optics that can achieve values of w and NA_{ray} less than or equal to 70% of the maximum allowable values.

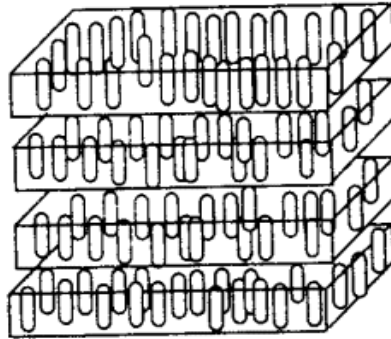
2.2 Liquid crystal spatial light modulator (LC-SLM) [45]

2.2.1 Three types of liquid crystal

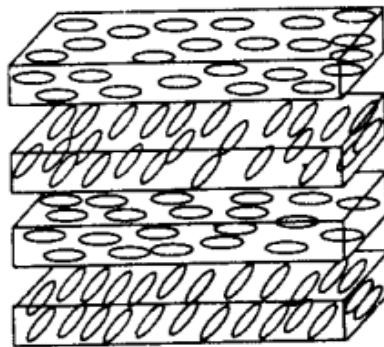
Liquid Crystal is a material between solid and liquid. General speaking, there are three kinds of phases of liquid crystals, known as smectic phase, nematic phase, and cholesteric phase. For the sake of clarity, we assume that the liquid crystals are made of rodlike molecules. A unit vector \mathbf{n} in the direction of the preferred orientation of the molecular axes is known as the director. Fig.2.4 (a) illustrates the nematic phase in which only a long range orientational order of the molecular axes exists. Fig.2.4 (b) illustrates the smectic phase in which one-dimensional translational order as well as orientational order exists. The cholesteric phase shown as Fig.2.4(c) is also a nematic type of LC except that it is composed of chiral molecules. As a consequence, the structure acquires a spontaneous twist about a helical axis normal to the director. The twist may be right-handed or left-handed depending on the molecular chirality.



(a)



(b)



(c)

Fig. 2-4 Three phases of liquid crystal:

(a) nematic phase (b) smectic phase (c) cholesteric pha

People can also control the director of nematic liquid crystal molecules by rubbing. This method is to coat a kind of liquid called polyimide inside the two pieces of glass, and then to brush the polyimide in the same direction. If we package nematic liquid crystal into these two pieces of glass, the director will parallel to the brushed direction. And the next liquid crystal molecules will follow the former molecule. Therefore the liquid crystal molecule's direction is decided by the two pieces of rubbed glass. When the two rubbed directions are perpendicular, the liquid crystal molecules will rotation in 90 degree from one side to the other side of the glass. It's called twisted nematic (TN) liquid crystal, which we applied in our system as a spatial modulator, and we will describe in detail later.

2.2.2 Principles of twisted nematic liquid crystal (normally black mode)

In our tunable optical demultiplexer system, we used the twisted nematic liquid crystal as a spatial light modulator (SLM). The spatial light modulator indicate that a modulator which can modulate amplitude or phase of a light in space. In order to control SLM by electric signal, we used twisted nematic liquid crystal as a wavelength selector. It has an advantage of electric and real time wavelength selecting.

Using the property of birefringence in twisted nematic liquid crystal molecules to modulate the light. Assume the liquid crystal molecule is an ellipsoid. The incident ray whose polarization state parallel to LC director is called extraordinary ray, and the refractive index is n_e ; The incident ray whose polarization state perpendicular to LC director is called ordinary ray, and the refractive is n_o . We can change the polarization of light by the twisted nematic liquid crystal (TN-LC) molecules, and it can be expanded by Jones' matrix.

Assuming a monochromatic ray whose wavelength is λ_0 incident to the liquid crystal has the polarization state as following:

$$\vec{V} = \begin{bmatrix} V_e \\ V_o \end{bmatrix} \quad (2.12)$$

where the V_e and V_o are the complex phasors in the e-direction and o-direction. The e direction is along the direction of the director in local principal coordinate system; the o direction is perpendicular to the direction of the director in local principal coordinate system. Because the director direction is the function of position, the TN-LC is not homogeneous. However we divide TN-LC plate into N equally thin plates. Thus each of the thin plates can be approximated by a homogeneous medium. Each plate is wave plate with a phase retardation and an azimuth angle. The overall Jones matrix can then be obtained by cascading these thin plate effect. Finally we obtain output polarization state through TN-LC by $N \rightarrow \infty$ and some calculations:

$$\vec{V}' = \begin{bmatrix} V_e' \\ V_o' \end{bmatrix} = \begin{bmatrix} \cos X - i \frac{\Gamma \sin X}{2X} & \phi \frac{\sin X}{X} \\ -\phi \frac{\sin X}{X} & \cos X + i \frac{\Gamma \sin X}{2X} \end{bmatrix} \begin{bmatrix} V_e \\ V_o \end{bmatrix} \quad (2.13)$$

Note $\begin{bmatrix} V_e' \\ V_o' \end{bmatrix}$ and $\begin{bmatrix} V_e \\ V_o \end{bmatrix}$ are polarization states in the local principal coordinate. Where the

parameter $X = \sqrt{\phi^2 + \left(\frac{\Gamma}{2}\right)^2}$, ϕ is total twist angle and the phase retardation

$\Gamma = \frac{2\pi}{\lambda_0}(n_e - n_o)d$, d is the thickness of TN-LC.

If we let TN-LC cell sandwiched between a pair of parallel polarizers whose transmission axis parallel to entrance local director.

Therefore the passed polarization is parallel to the director of LC at the entrance plane. In the local principal coordinate system, the input polarization state after the front polarizer can be written as the following Jones vector:

$$\vec{V} = \begin{bmatrix} V_e \\ V_o \end{bmatrix} = \frac{1}{\sqrt{2}} \begin{bmatrix} 1 \\ 0 \end{bmatrix} \text{ for unpolarized light incident} \quad (2.14)$$

The output polarization state before the second polarizer in terms of the Jones vector in the local principal coordinate at the exit plane can be written, according to Eq.(2.), as follows:

$$\vec{V}' = \begin{bmatrix} V_e' \\ V_o' \end{bmatrix} = \frac{1}{\sqrt{2}} \begin{bmatrix} \cos X - i \frac{\Gamma \sin X}{2X} & \phi \frac{\sin X}{X} \\ -\phi \frac{\sin X}{X} & \cos X + i \frac{\Gamma \sin X}{2X} \end{bmatrix} \begin{bmatrix} 1 \\ 0 \end{bmatrix} = \frac{1}{\sqrt{2}} \begin{bmatrix} \cos X - i \frac{\Gamma \sin X}{2X} \\ -\phi \frac{\sin X}{X} \end{bmatrix} \quad (2.15)$$

After passing the second polarizer, the final polarization state will be:

$$\vec{V}'' = \begin{bmatrix} V_e'' \\ V_o'' \end{bmatrix} = \frac{1}{\sqrt{2}} \begin{bmatrix} 0 & 0 \\ 0 & 1 \end{bmatrix} \begin{bmatrix} \cos X - i \frac{\Gamma \sin X}{2X} \\ -\phi \frac{\sin X}{X} \end{bmatrix} = \frac{1}{\sqrt{2}} \begin{bmatrix} 0 \\ -\phi \frac{\sin X}{X} \end{bmatrix} \quad (2.16)$$

Then total transmission T will follows as:

$$T = \frac{1}{2} \phi^2 \left(\frac{\sin X}{X} \right)^2 = \frac{1}{2} \phi^2 \frac{\sin^2 \left(\phi \sqrt{1 + \left(\frac{\Gamma}{2\phi} \right)^2} \right)}{\phi^2 \left[1 + \left(\frac{\Gamma}{2\phi} \right)^2 \right]} = \frac{1}{2} \frac{\sin^2 [\phi \sqrt{1 + u^2}]}{1 + u^2} = \frac{1}{2} \frac{\sin^2 \left[\frac{\pi}{2} \sqrt{1 + u^2} \right]}{1 + u^2} \quad (2.17)$$

(2.17)

where u called Mauguin parameter is defined as:

$$u \equiv \frac{\Gamma}{2\phi} = \frac{2}{\lambda_0} (n_e - n_o) d \text{ for total twist angle } \phi \text{ is } \frac{\pi}{2} \quad (2.18)$$

We plot the transmission formula Eq.(2.17) as a function of the parameter u in Fig. 2.5.

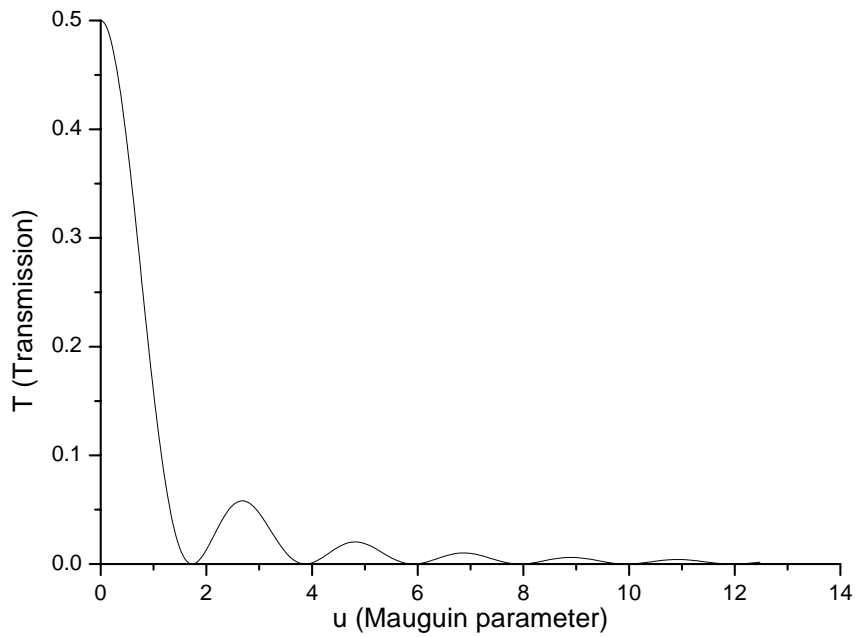


Fig. 2-5 Transmission versus Mauguin parameter u

In above situation the design, the 90° TN cell sandwiched between a pair of parallel polarizers, is called Normally black (NB) mode. For LC E_7 material at $\lambda_0 = 1550 \text{ nm}$, $n = n_e - n_o = 0.225$. We also plot T as a function TN-LC thickness in Fig.2-6.

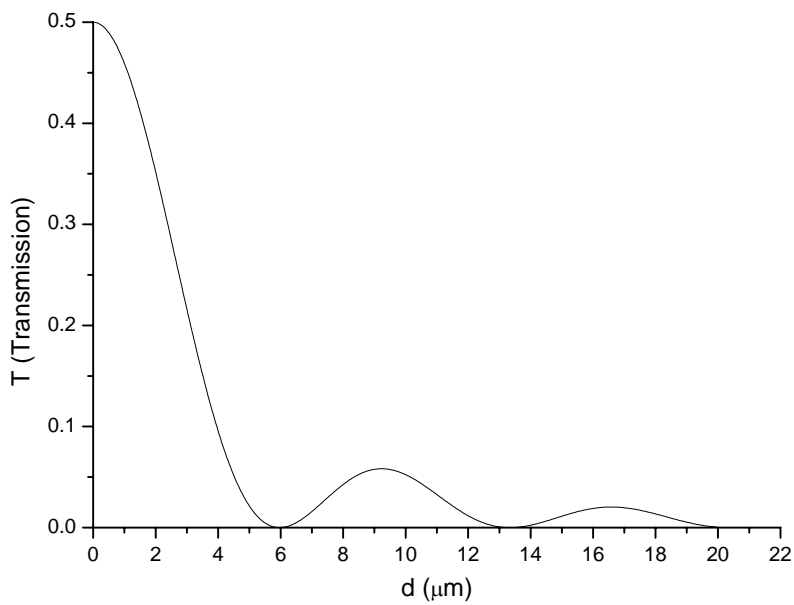


Fig. 2-6 Transmission versus thickness d (μm)

From Fig. 2-6. we select first transmission minimum point, which representing thickness $d=6 \mu\text{m}$ ($u=1.742$), in order to achieve NB mode (LC off state). Note (2.15) become $\vec{V}' = \begin{bmatrix} V_e' \\ V_o' \end{bmatrix} = \frac{1}{\sqrt{2}} \begin{bmatrix} \cos X \\ 0 \end{bmatrix}$ when d is small than . In other words, the polarization through TNLC cell is perpendicular to the second polarizer. Thus the transmission will be zero through the second polarizer.(LC off state; see Fig. 2-7 (a))

Consider special condition, however, often happens in TN-LC that the total twist angle is much smaller than the phase retardation angle .

The Eq.(2.15) becomes $\vec{V}' = \begin{bmatrix} V_e' \\ V_o' \end{bmatrix} = \frac{1}{\sqrt{2}} \begin{bmatrix} e^{-i\frac{\Gamma}{2}} \\ 0 \end{bmatrix}$ which is independent of

under assumption of \ll (or u is a large number) and T will be zero . In other words, the electric field vector of the beam remains parallel to the local director as the beam propagates in the twisted nematic LC medium and blocked by second polarizer. This explains the phenomenon of adiabatic following (or waveguiding). Obviously it is also shown in Fig. 2-5 when u is large.

On the contrary, if the two polarizers are cross, the incident ray will pass through the second polarizer. And this kind of twisted nematic liquid crystal device is called Normally White (NW). In tunable optical demultiplexer system, we operate in NB mode. Because first order diffracted light was polarized by grating, we just need one polarizer to fabricate our twisted nematic liquid crystal spatial modulator.

When applying a large enough AC electric field on two electrodes, the almost all directors will be tilt 90^0 toward the electric field except for those adjacent to the polyimide surfaces shown as Fig 2-7 (b). Thus light passing through the TN-LC will see the refraction index, n_0 , only and

polarization of light will not change. In normally black mode, the light will pass through the rear polarizer when applying a large enough AC electric field (LC on state; see Fig.2-7 (b)).

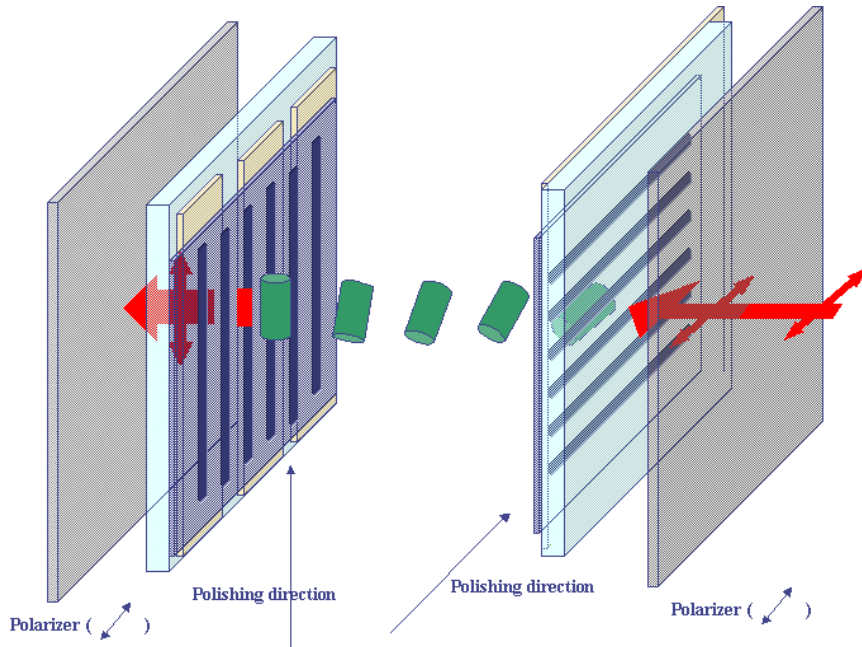


Fig. 2-7(a) Polarization of the light incident on the LC-SLM from the left will be blocked by the LC-SLM if the driving voltage was turned off.

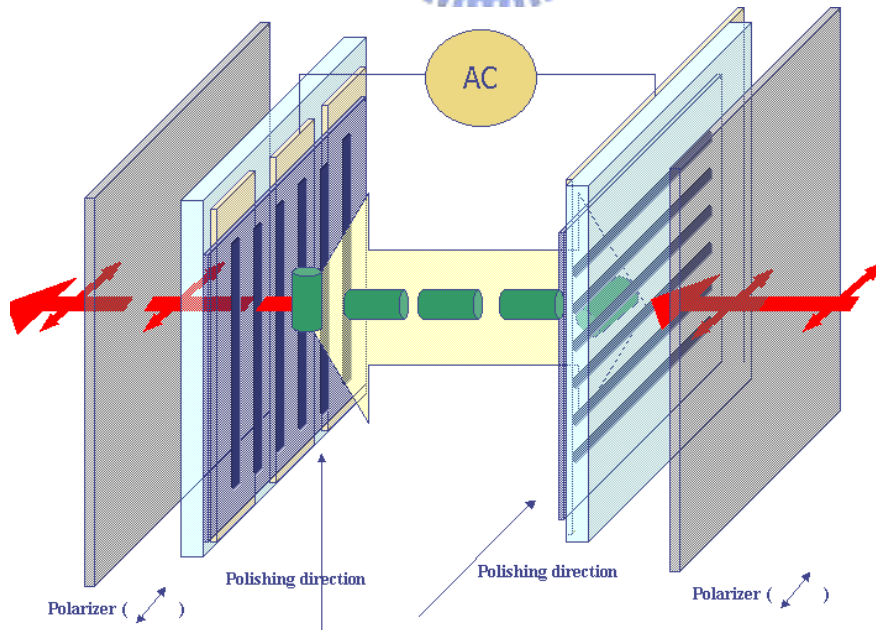


Fig. 2-7(b) Polarization of the light incident on the LC-SLM from the left will pass through the LC-SLM if the enough large driving voltage was turned on.

2.2.3 Construction of the LC-SLM

Our LC-SLM's was assisted by ITUI and EP-NCTU. The constructions of LC-SLM's is similar. Details of the fabrication processes can be found in Chrong-Hann Niou's thesis [46]. A brief summary is given below.

Fig. 2-8 illustrates the structure of original design of TNLC spatial modulator. The TNLC was packaged by two pieces of glass coated indium tin oxide (ITO) as transparent electrodes. The ITO layer on the rear glass had been etched into the desired pattern by semiconductor process. The ITO layer on the front glass is the common electrode. The rear polarizer is attached behind the rear glass. The thickness of TNLC layer is about 6 μm .

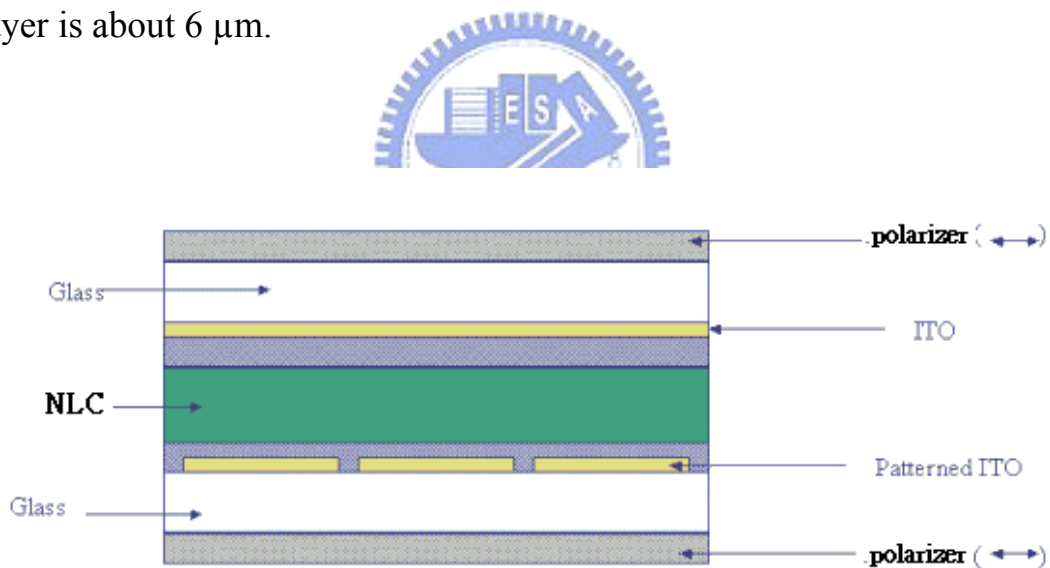


Fig. 2-8 Structure of homemade TNLC (original design) spatial modulator. ITO: Indium Tin Oxide, NLC: Nematic Liquid Crystal

We designed a LC ITO pattern in order to match the fiber array whose pitch is 250 μm and commissioned ITRI to fabricate LC devices shown in Fig 2-9.

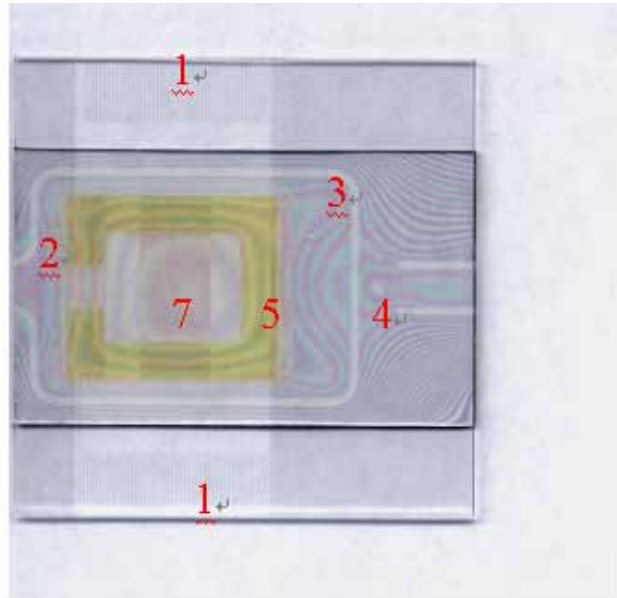


Fig. 2-9 TN-LC (new design) device

The ITO pattern of design is shown in Fig.2-10(a)(b). Each has 92 independent pixels. There are 46 terminal pixels at each edge interface and each pixel linewidth is $220\ \mu\text{m}$ and spacing between the two pixels is also $220\ \mu\text{m}$. These terminal pixels are bound with flat flexible cables (FFCs) connected the electrical controlled board. Each pixel linewidth is $125\ \mu\text{m}$ and spacing between the two pixels is $25\ \mu\text{m}$ in center area of another pattern (The pixel pitch is $125\ \mu\text{m}$). Fig. 2-10 (c) shows the picture of real object.

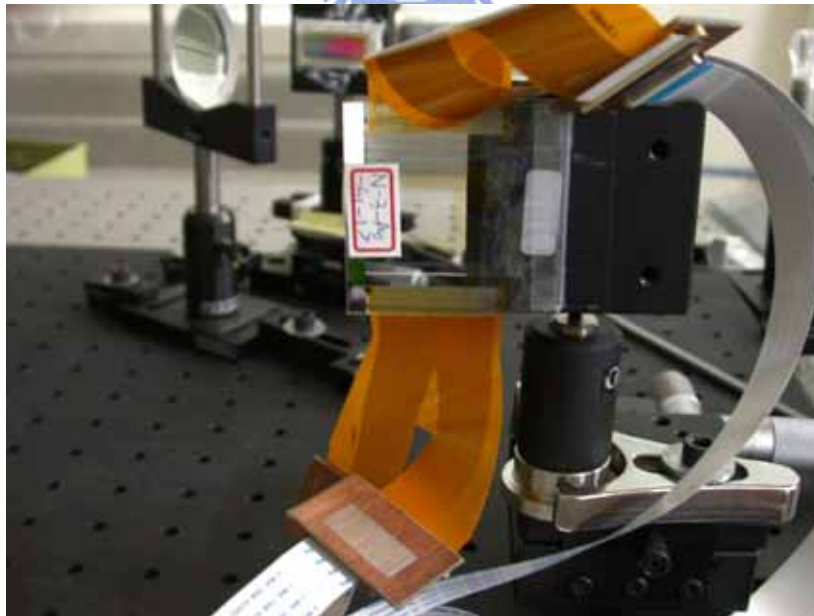
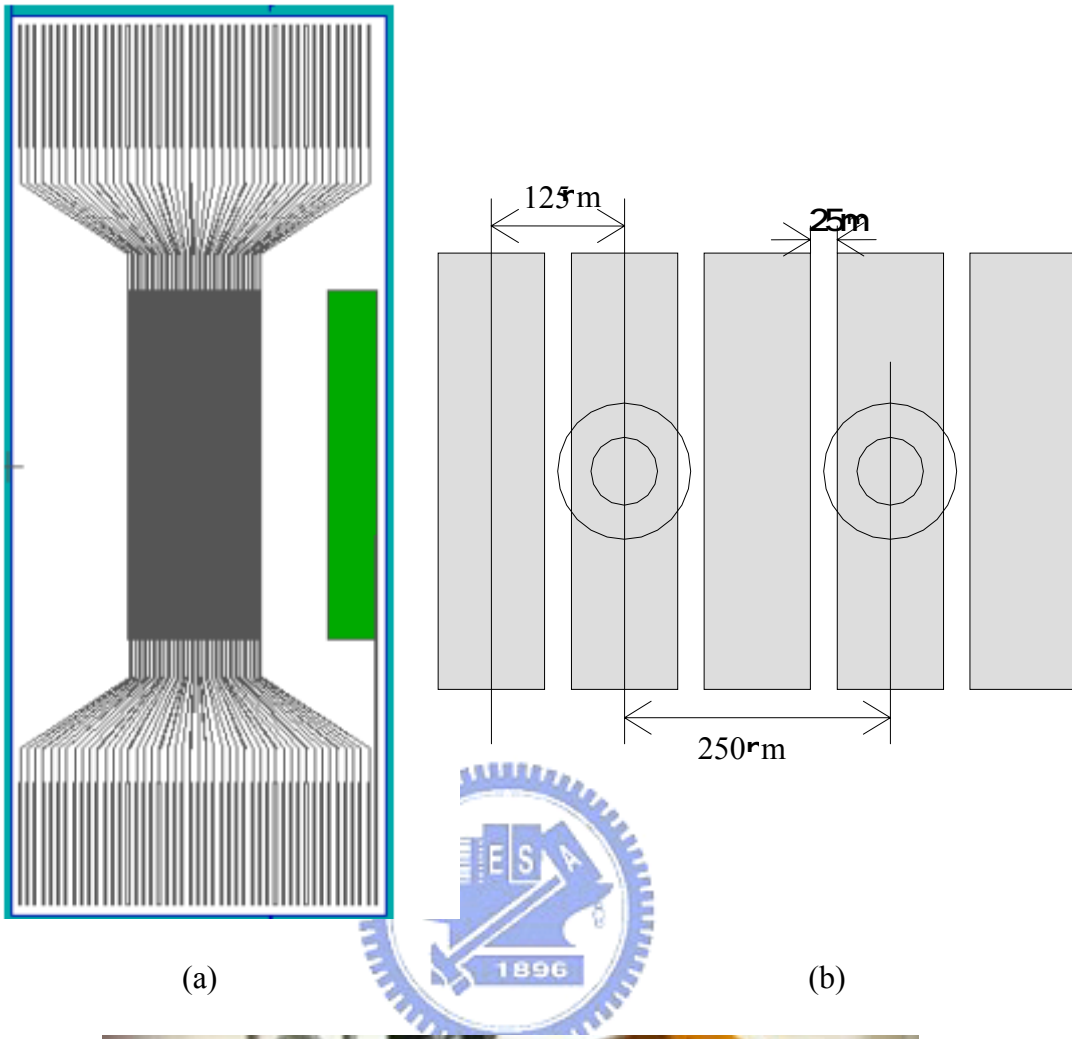


Fig. 2-10 (a) (b) ITO pattern of TNLC device (c) picture of real object

Now we describe the LC devices shown in Fig 2-10 in detail. Each position is shown as its corresponding number:

1. *Edge interface*: 46 terminal pixels are located here. Each pixel linewidth is 220 μm and spacing between the two pixels is also 220 μm .
2. *LC injection entrance*: We inject LC into the device at here.
3. *Flame glue*: there are so many polymer balls whose diameter is 6.2 μm .
4. *Silver glue*: It is used to conduct common board.
5. *Photoresistors*: They are used to determine the device thickness. The thickness is about 6 μm .
7. *Center area*: The pixels work region is located here. The pixel pitch is 125 μm . Each pixel linewidth is 100 μm and spacing between the two pixels is also 25 μm .



2.3 Fiber array

Fiber array is made by sandwiching optical fibers to a pair of precisely spaced V-groove blocks. The V-grooved blocks are obtained by state of art micro-fabrication process either anisotropic etching or precision grinding. High pitch position accuracy is required for alignment between single or multi-channel optoelectronic devices. Fiber Arrays have angle-polished end-faces and can be used for coupling to many kinds of PLC application devices such as AWG, Splitter, MEMS switch, integrated optical device, and arrayed detector. Our fiber arrays are made from micro-machined Quartz or Pyrex T, which provide excellent fiber-to-fiber pitch and planarity. The Quartz V-groove has the same coefficient of thermal expansion with Optical fiber, UV-transparency, and high durability. Our fiber arrays are made from micro-

machined Quartz or Pyrex T , which provide excellent fiber-to-fiber pitch and planarity. The Quartz V-groove has the same coefficient of thermal expansion with Optical fiber, UV-transparency, and high durability.

2.3.1 Fiber array's Characteristics

(1) Number of channels

The channel spacing is a straightforward parameter, how many channels can place in the V-groove. Popular channels in the fiber array have 1, 2, 4, 8, 16, 32, 48 and 80. In our experiment it's 16.

(2) Channel Spacing

The channel spacing, which is the length between channels in the V-groove that is required to guarantee minimum crosstalk degradation. Popular spacing in the fiber array have 127 and 250 μ m. In our experiment it's 250 μ m.

(3) Fiber type

We know that as a pulse travels down a fiber, dispersion causes pulse spreading. This limits the distance and the bit rate of data on an optical fiber. So there are two type fibers, one is single mode fiber, is 9/125 μ m; another is multi-mode fiber, is 50/125 and 62.5/125 μ m. In our experiment we need to collect more, it's a 62.5/125 multi-mode fiber.

(4) Structure

The structure, which is construction of V-groove packed the fibers in the Si or glass regularly. There are three types of structure, Single V/Full coverage, Single V/Half coverage and Double V/Full coverage. Our fiber

array is Single V/Full coverage.

(5) End face polish

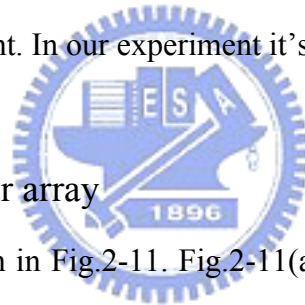
The connector endface preparation will determine what the connector return loss, also known as back reflection, will be. Flat Polish (0 degree), a flat polish of the connector surface will result in a back reflection of about -16dB (4%). APC Polish (± 8 degree and ± 12 degree popularly), adds an 8 degree angle to the connector endface. Back reflections of $< -60\text{dB}$ can routinely be accomplished with this polish. In our experiment, we don't care about the reflection. It's a zero degree face polish.

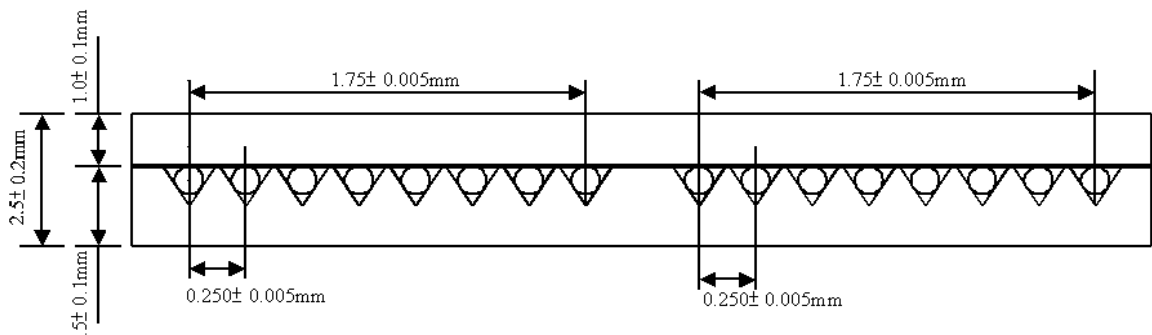
(6) Number of fiber per ribbon

In order to marshal those fibers, will be make up the ribbon. The number of fibers/ribbon has four and eight. In our experiment it's 8 fibers/ribbon.

2.3.2 The data of our Fiber array

The fiber array is shown in Fig.2-11. Fig.2-11(a) show a lateral view, there are 16 channels, $250\ \mu\text{m}$, 62.5/125 multi-mode fiber, Single V/Full coverage, zero degree face polish, and 8 fibers/ribbon in our fiber array. Fig.2-11(b) show the picture of real object.





(a)



(b)

Fig. 2-11 Structure of Fiber array (a) real device structure - side view fig (b) picture of real object

Chapter 3

Optical Demultiplexer with Liquid Crystal

Experiments and Results

In this chapter we describe the basic design concept of tunable optical demultiplexer using liquid-crystal-based device and demonstrate the experimental results.

3.1 Basic optical demultiplexer experiments without LC-SLM

Fig 3-1 shows the basic demultiplexer configuration including a commercially available Erbium Doped Fiber Amplifier used as the broadband light source. The EDFA connect single mode fiber output was collimated to a parallel beam of light by an collimating lens (Burleigh), then incident on the grating (Agilent 1100 *lines/mm* with $\theta_i=85^\circ$) after a linear polarizer (Corning polarcor, AR coating @ 1550nm, T=97.5%, extinction ratio > 30 dB) with the diffracted angle $\theta_r=44.25^\circ$ for $\lambda=1540$ nm. The spectrally dispersed beam directly collected by the AR-coating lens (diameter=50.8 mm; f=205.5mm) and then focused on lens focal plane. The fiber array is placed on focal plane to collect the different wavelength into their corresponding fiber. Fig. 2-12 except fiber array structure. Our fiber array is consisted of 16 multimode fibers (core diameter=62.5 μm ; cladding diameter=125 μm), which are divided into 2 groups. The group spacing is 500 μm (500 $\mu\text{m} \pm 0.5$). Eight fiber elements are equally spaced 250 μm . In other words, the Core pitch is 250 μm (250 $\mu\text{m}\pm 0.5$). Finally we selected one fiber of fiber array to observe the collected spectrum from OSA (Advantest Q8384, resolution 0.01nm). The

spatial dispersion relation ($d\lambda/dx$) is 3.16871 (nm/mm) or 0.792178 (nm/250 μ m) for $\lambda=1540$ nm.

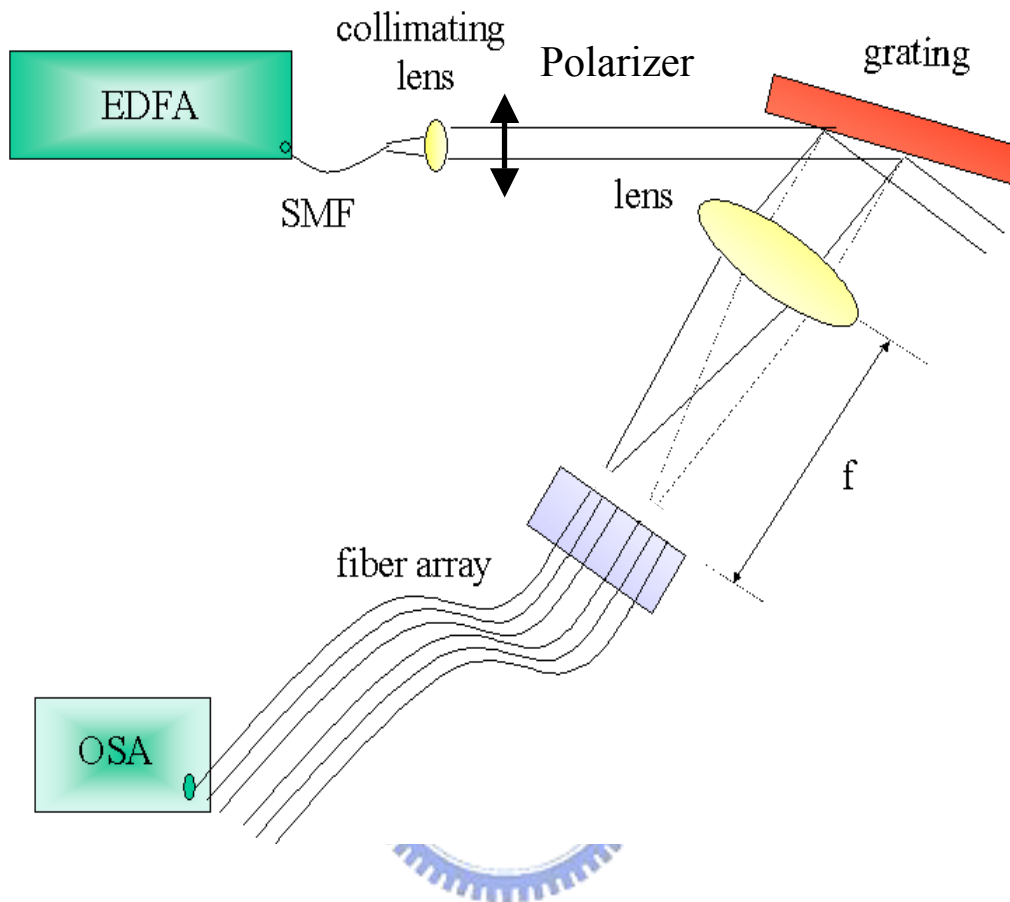


Fig. 3-1 Basic demultiplexer system. OSA: Optical Spectrum Analyzer

The ASE spectrum of EDFA is shown in Fig. 3-2. The ASE source can cover from 1525 to 1560 nm, with a total power of 15.7 dBm, and its light is unpolarized.

Fig. 3-3 shows the collected spectrum curve at the fiber array on the focal plane when input source is EDFA ASE with P and S-state polarizations. The channel peak power obviously suffered from EDFA ASE input power. The fiber array each channel step is 250 μ m and the spectral step between 8th and 9th is 500 μ m. We let one of ITU grid wavelengths (1540.56 nm) become center wavelength of the 9th channel fiber by adjusting the fiber array along the focal plane. Our grating is polarization sensitive, the p-state linear polarization input light incident on the grating. The grating provides

greater diffraction efficiency more than s-state linear polarization input light. Their output power difference is about 15 dB. We can clearly see that the total crosstalk of adjacent channel is less than -30 dB obviously except the 16th channel. Fig. 3-4 shows the comparison between experimental results and theoretical curve. The results are matched with theoretical curve.

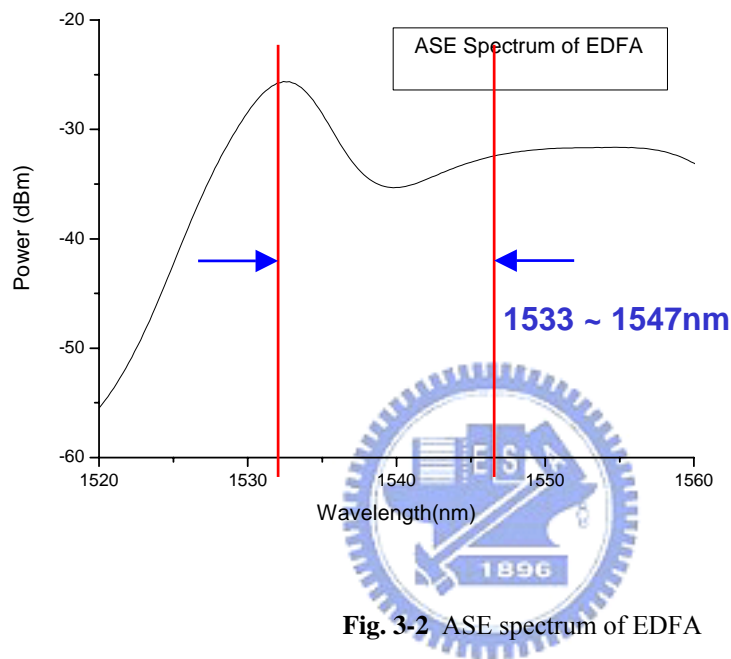


Fig. 3-2 ASE spectrum of EDFA

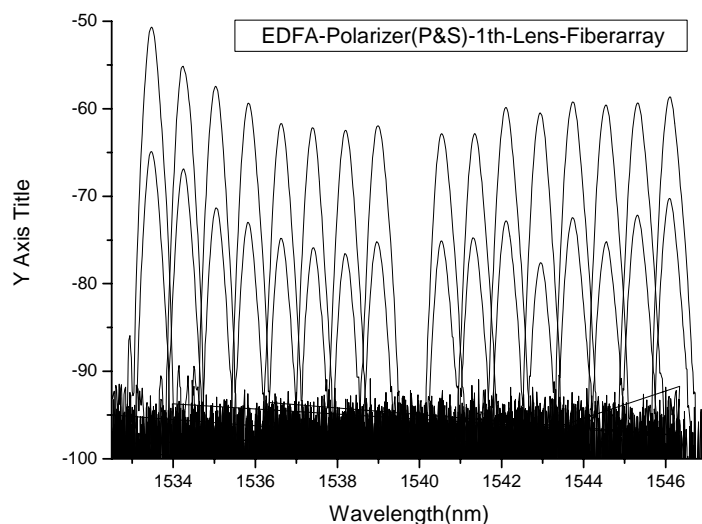


Fig. 3-3 Basic demultiplex of spectrum using EDFA of P and S state polarizations. The center wavelength of each channel almost equals to ITU grid (spacing=100Ghz)

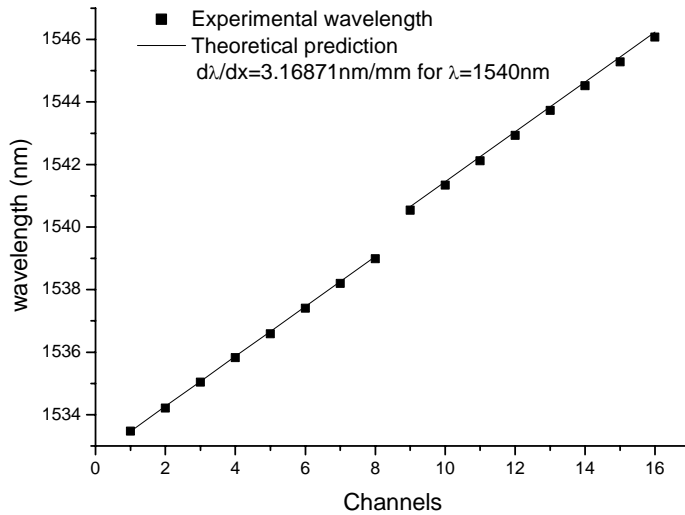


Fig. 3-4 Comparison between optical demultiplexer/filter experimental results and theoretical curve.

Theoretical and experimental channel spacing are 0.792 nm.

3.2 Optical Demultiplexer with LC-SLM

3.2.1 Transmittance of the LC-SLM

We measure the transmission curve of the LC-SLM when varying the ac voltage across it. The experiment was accomplished by Ming-Chieh Huang. The measurement system is shown schematically in Fig. 3-5. It was configured in a Littman extended-cavity arrangement. The output light of the LD was collimated by an objective lens of 0.47 numerical aperture, then incident on a diffraction grating (Agilent 1100 lines/mm) at an angle of 80°. Spectrally selective optical feedback was provided by the retro-reflected first-order-diffracted light from the mirror. The zero-order reflection from the grating is the laser output.

The polarization of the output light of the Littman laser is rotated to the appropriate direction by a half wave plate and focused on a pixel of the TNLC by an objective lens (Newport F-L20B). Then the light is collimated and focused on the power meter. The structure of the LC-SLM was described in chapter 2. The pixel

pitch of LC-SLM is 105 μm and the pixel width of it is 100 μm . And the thickness of the LC-SLM layer is about 8 μm . We measured the transmission curve when varying the ac voltage across the LC-SLM cell. The transmission result is shown in Fig.3-6. The saturation transmission is about 76~80 % when V_{rms} is larger than 3.5 Volt from Fig. 3-6.

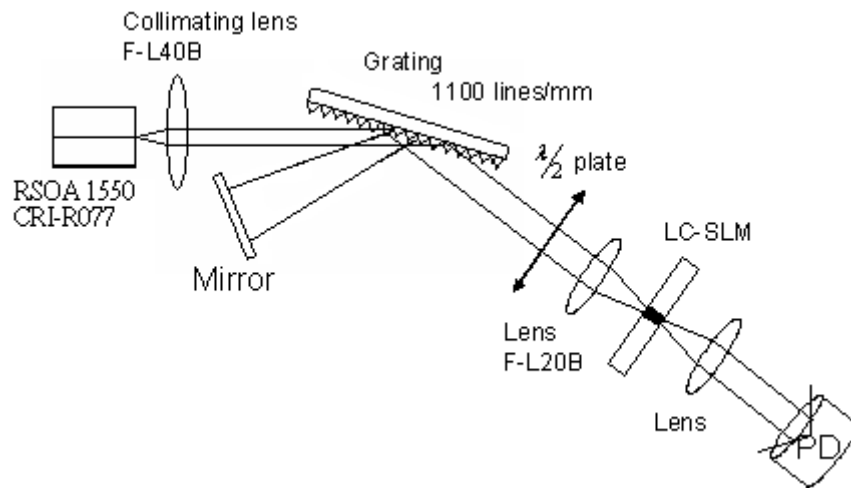


Fig. 3-5 The measurement setup of transmission of the TNLC

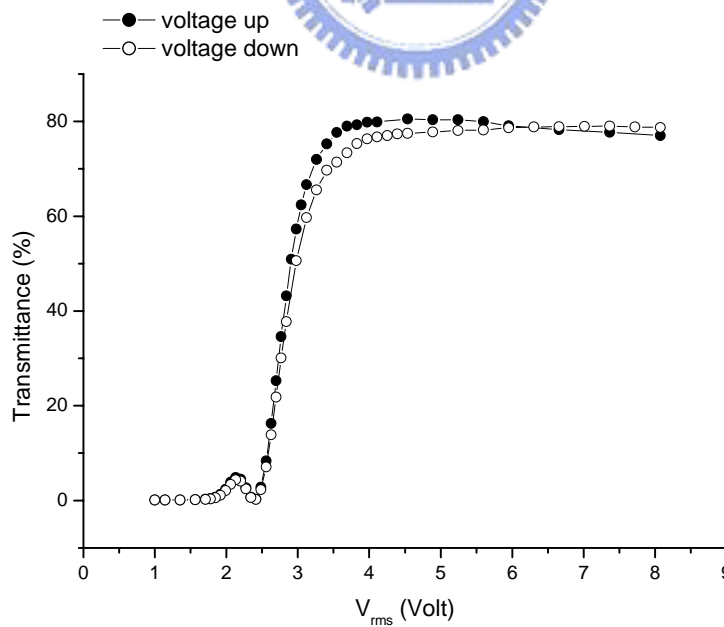


Fig. 3-6 The transmission curve of the TNLC cell detected by power meter.

Solid line: voltage down; dash line: voltage up

3.2.2 Tunable Optical Demultiplexer experiment of P-state polarization with LC-SLM

The tunable optical demultiplexer setup shown in Fig.3-7 is roughly the same as described above (see Fig.3-1) besides arranging LC-SLM (pixel pitch=125 μm ; pixel width =100 μm ; thickness=8 μm). The LC-SLM is tightly closed to fiber array. Every pixel of LC-SLM is corresponding to every fiber element of fiber array one by one. We can see Fig. 2-10 (b).

Fig. 3-8 shows the 16th channel pixel on-off spectrum of tunable optical demultiplexer P-state polarization with LC-SLM. Each channel on-off performance is shown in Fig. 3-9. The extinction ratio ranges from 11.1 dB to 16.2 dB. The average extinction ratio is 13.5 dB. From Fig.3-8 and 3-9, we see that the each channel pixel-on power level is -54 dBm to -64 dBm and pixel-off power level is -68dBm to -81 dBm. Then we vary the LC-SLM input voltage to modulate the each channel transmittance to -65 dBm. The received normalized spectrum of optical demultiplexer is shown in Fig. 3-10. We get a beautiful spectrum, the variation between different channels are reduced ~ 10 dB to less than 0.5dB. Fig. 3-11 shows the EDFA source and Pixel on; off and normalized power with P-state polarization.

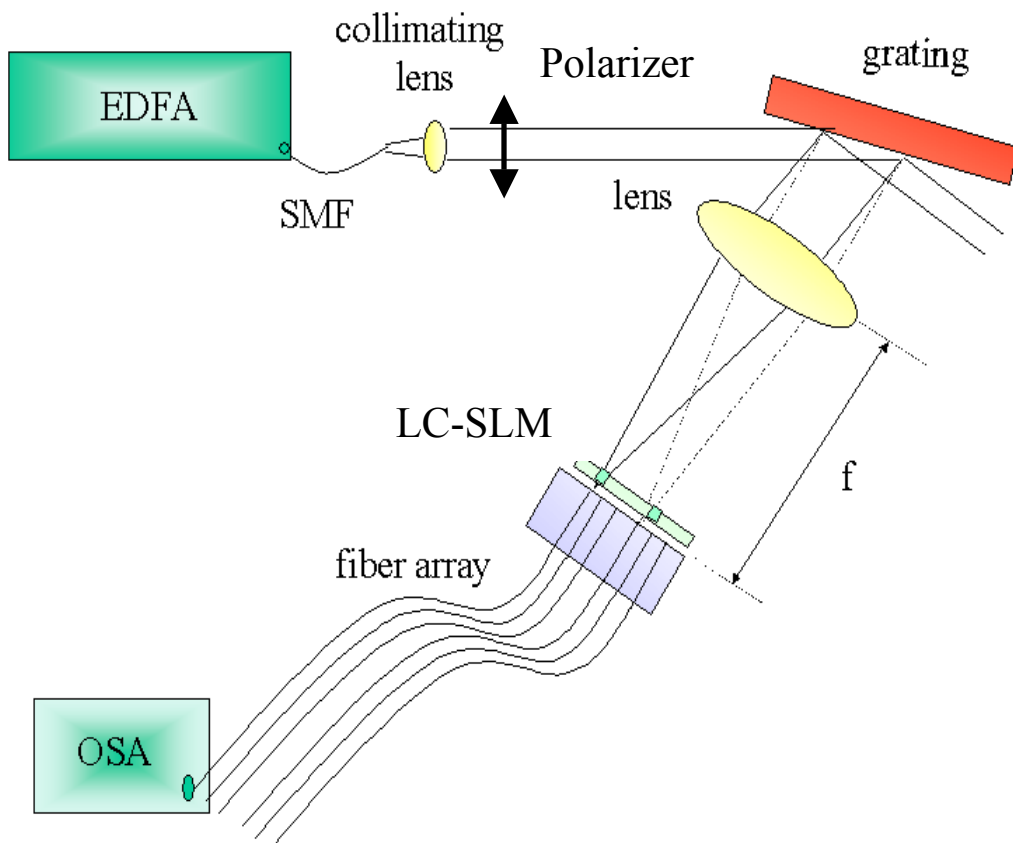


Fig. 3-7 Tunable optical demultiplex of spectrum of P-state polarization and LC-SLM is all pixel on and off. The center wavelength of each channel almost equals to ITU grid (spacing=100Ghz)

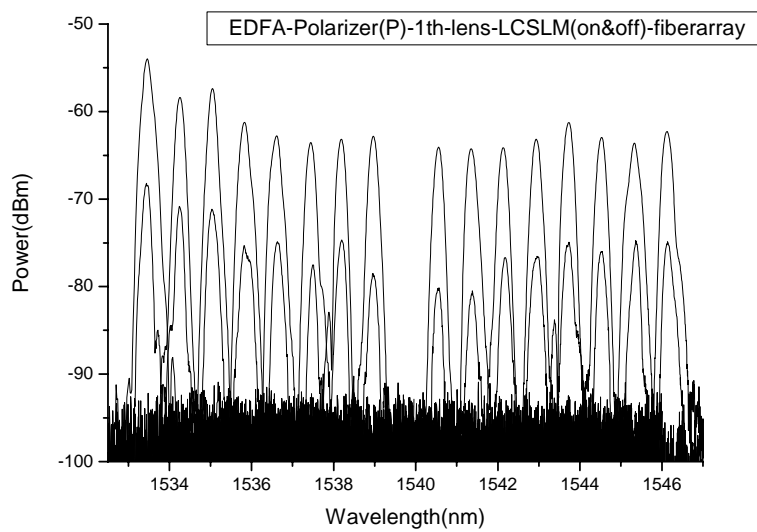


Fig. 3-8 Tunable optical demultiplex of spectrum of P-state polarization and LC-SLM is all pixel on and off. The center wavelength of each channel almost equals to ITU grid (spacing=100Ghz)

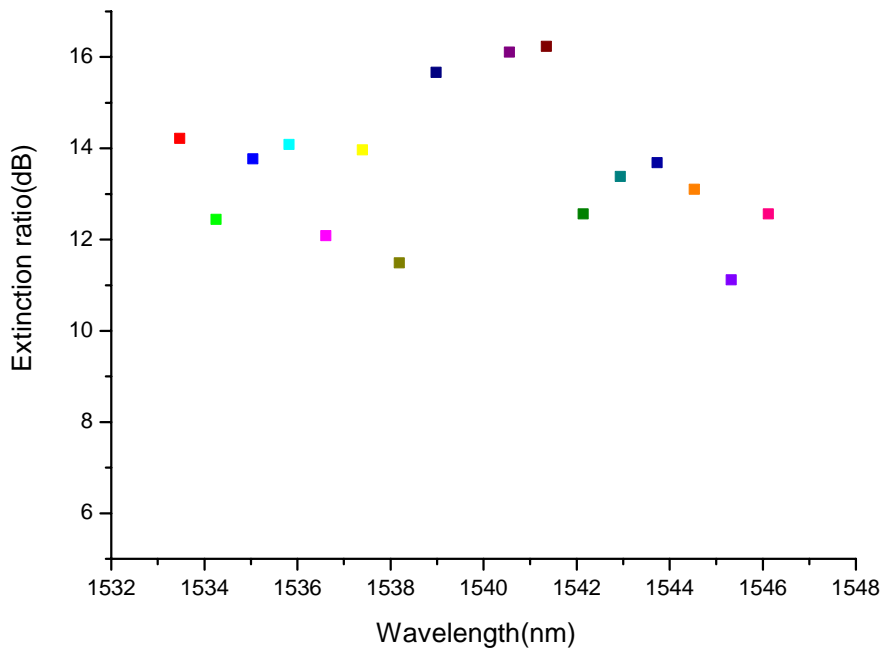


Fig. 3-9 Extinction ratios of the individual channels versus wavelength_with P-Polarization

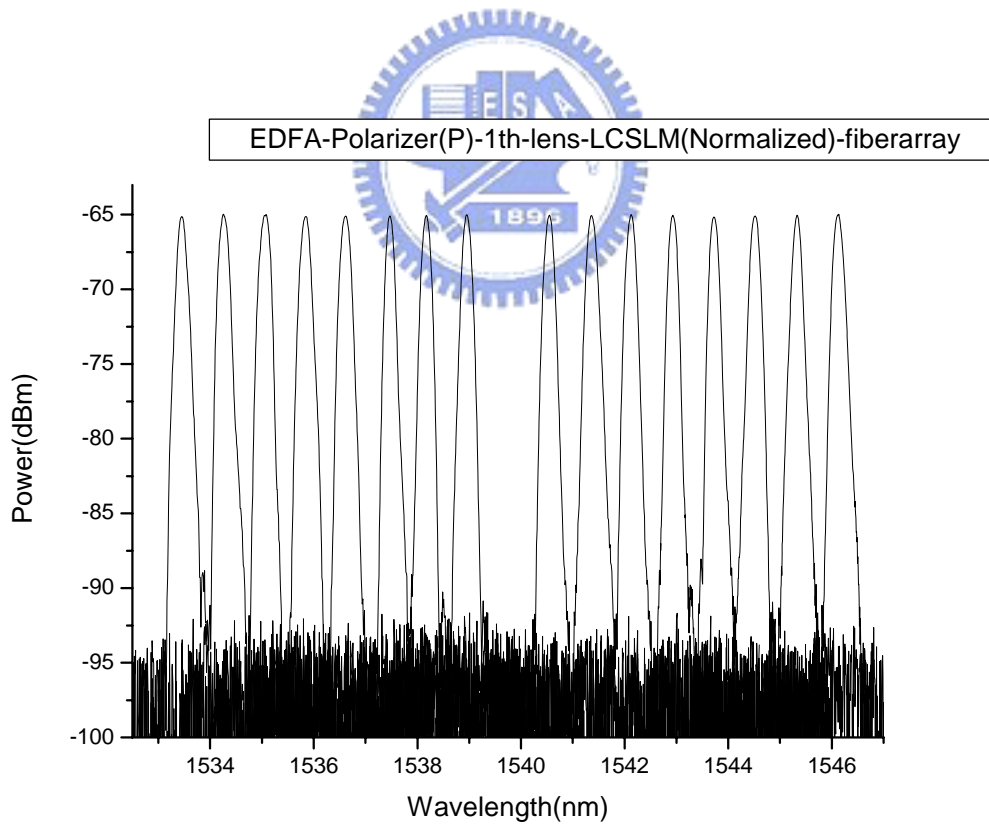


Fig. 3-10 Tunable optical demultiplex of spectrum of P-state polarization and LC-SLM is all equalize to -65 dBm. The center wavelength of each channel almost equals to ITU grid (spacing=100Ghz)

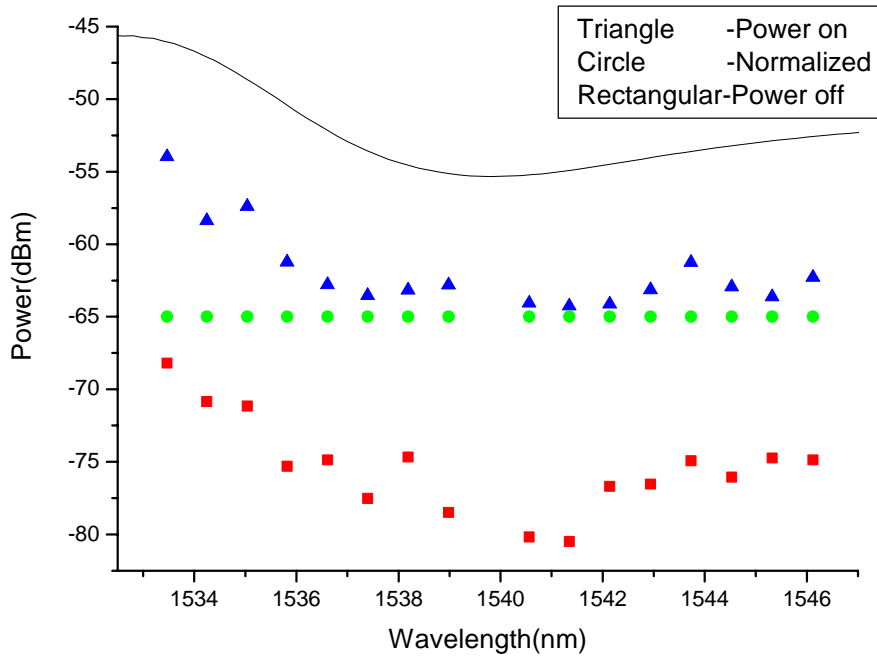


Fig. 3-11 The EDFA source and Pixel on; off and normalized power with P-state polarization

3.2.3 Tunable Optical Demultiplexer experiment of S-state polarization with LC-SLM

Because of our experiment device grating is polarization sensitive component, the different state polarizations incident the grating and then get the different power level. The present grating device is polarization sensitive with a polarization dependent loss (PDL) of about 15 dB.

For our LC-SLM component, if the two polarizers are cross, the incident ray will pass through the second polarizer. And this kind of twisted nematic liquid crystal device is called Normally White (NW). It's the same with the optical demultiplexer of S-state polarization. When applying a large enough AC electric field except for those the LC-SLM pixels, the transmittance will be reduce. It's pixel-on.

Fig. 3-12 shows the 16th channel pixel on-off spectrum of tunable optical demultiplexer S-state polarization with LC-SLM. Each channel on-off performance is

show in Fig. 3-13. The extinction ratio ranges from 6.7 dB to 13.1 dB. The average extinction ratio is 10.1 dB. Form Fig.3-12 and 3-13, we see that the each channel pixel-on power level is -68 dBm to -79.5 dBm and pixel-off power level is -80.5 dBm to -91.1 dBm. Then we vary the LC-SLM input voltage to modulate the each channel transmittance to -80 dBm. The received normalized spectrum of optical demultiplexer is shown in Fig. 3-14. The variation between different channels are reduced ~ 10 dB to less than 1.1dB. Fig. 3-15 shows the Pixel on; off and normalized power with S-state polarization.

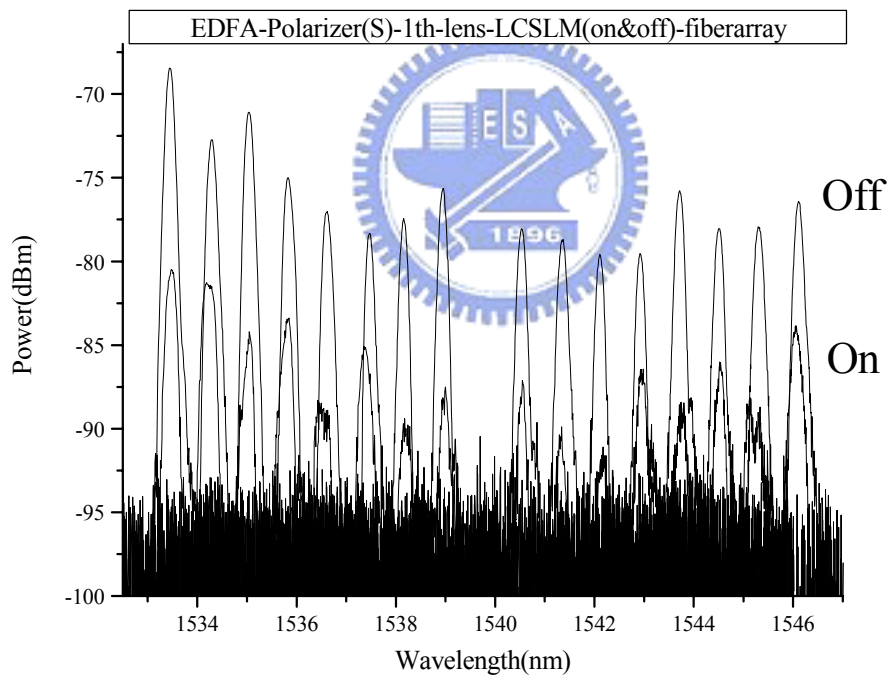


Fig. 3-12 Tunable optical demultiplex of spectrum of S-state polarization and LC-SLM is all pixel off and on. The center wavelength of each channel almost equals to ITU grid (spacing=100Ghz)

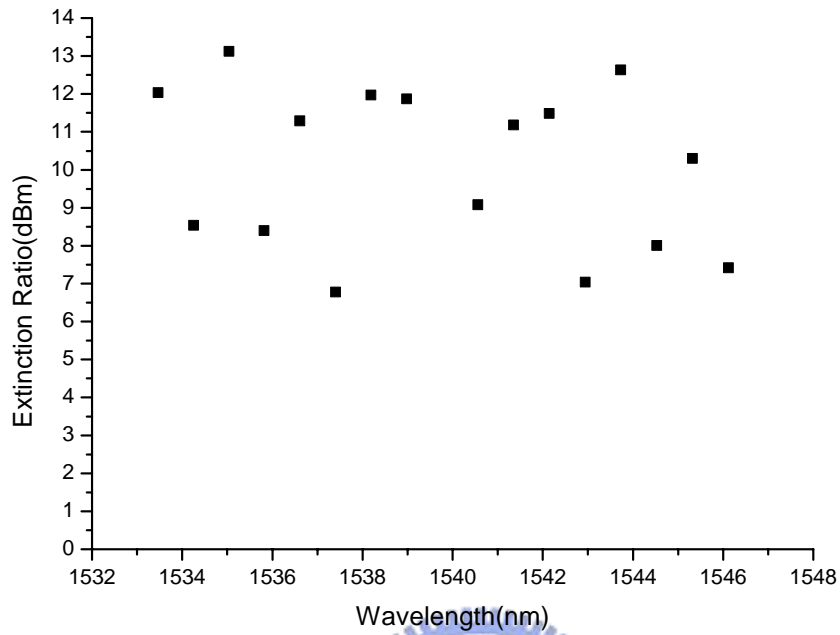


Fig. 3-13 Extinction ratios of the individual channels versus wavelength_with S-Polarization

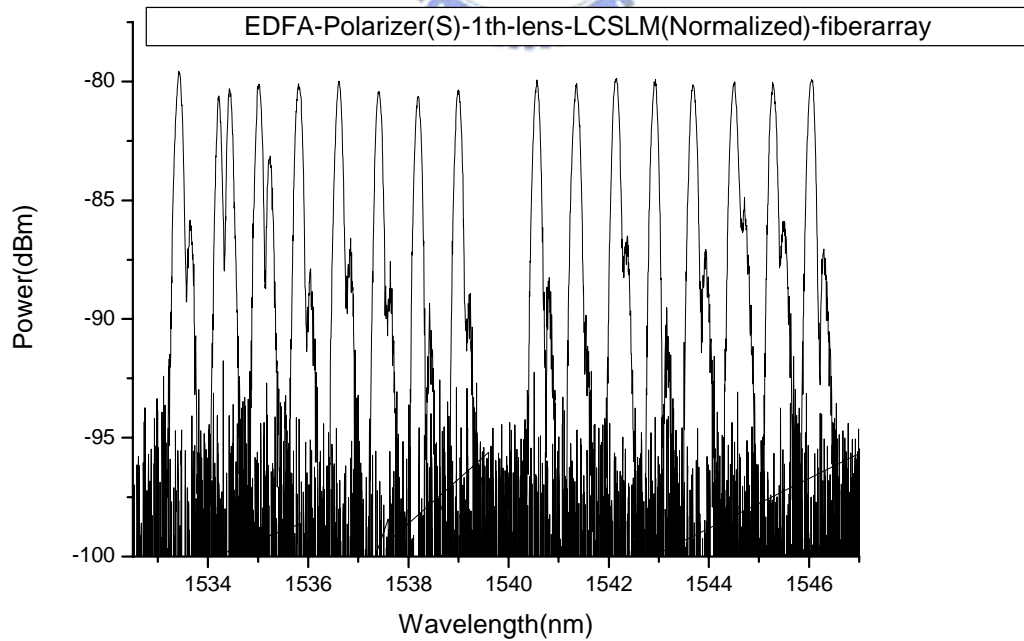


Fig. 3-14 Tunable optical demultiplex of spectrum of S-state polarization and LC-SLM is all equalize to -80 dBm. The center wavelength of each channel almost equals to ITU grid (spacing=100Ghz)

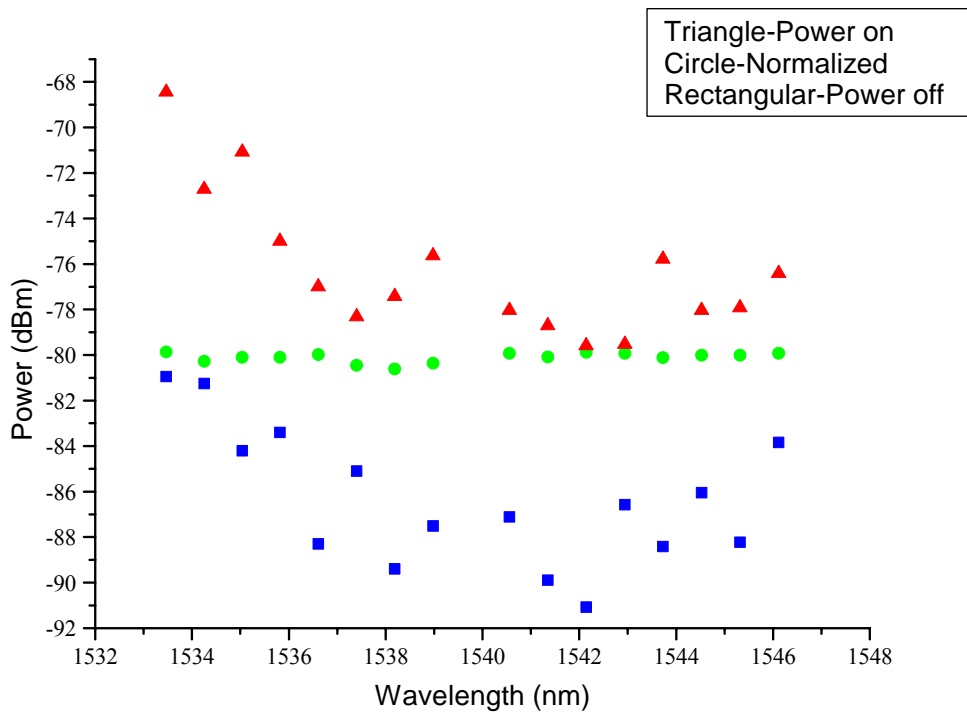


Fig. 3-15 Pixel on; off and normalized power with S-state polarization



3.3 Tunable Optical Demultiplexer experiment discussion and summary table

The output spectra of the 16-channel power equalized LC-multi-DEMUX for both s and p polarizations are shown in Fig. 3-16. The present device is polarization sensitive with a polarization dependent loss (PDL) of about 15 dB. It can be improved by using a polarization-insensitive grating and polarization independent polymer dispersed LC (PDLC) for the LC-SLM.

The output wavelengths of the channels are in good agreement with the theoretical prediction according to Eq. (2.10) and the ITU wavelengths (within 0.04 nm or 5 GHz). The crosstalk of adjacent channels is less than – 30 dB. The average

1dB and 3dB passbands of the DEMUX are 12.5 and 22.5 GHz, respectively. The IL for the LC-multi-DEMUX prototype is approximately 12 dB, which includes 3-dB loss of the unpolarized light from the EDFA. The losses incurred on signal light propagating through the collimating lens, grating, lens and LC-SLM are 0.7 dB, 1.5 dB, 1 dB and 3 dB respectively. The remaining loss is attributed to that of coupling into the fiber array. We expect the best achievable IL for the LC-multi-DEMUX to be about 5 dB.

As the pixels can be individually switched on/off and the transmission of the particular channel adjusted, the LC-multi-DEMUX has additional functionalities as compared to conventional DEMUXs. The outputs of the channels are equalized to -65 dBm. The variation between different channels are reduced from ~ 10 dB to less than 0.5 dB. The pixel-on-off characteristics of the 16 channels of the LC-multi-DEMUX are shown in Fig. 3-9. The extinction ratios for pixels on/off for the 16 channels range from 11.1 dB to 16.2 dB. The average extinction ratio is 13.53 dB. We have employed polarization optics with extinction ratios of 10^5 . The extinction ratio of the LC-multi-DEMUX is theoretically better than 30 dB, but depends critically on the thickness of the LC layer. Thus the extinction ratios of different channels of our home-made LC-multi-DEMUX fluctuate because the thickness of the LC-SLM is not uniform across the channels.

The design concept of the present device can be extended readily to other grating-based DEMUXs, which employ either echelle gratings or array waveguide grating as the dispersion elements.

We show the summary data **Table 3-1** for the 16-channel LC-multi-DEMUX.

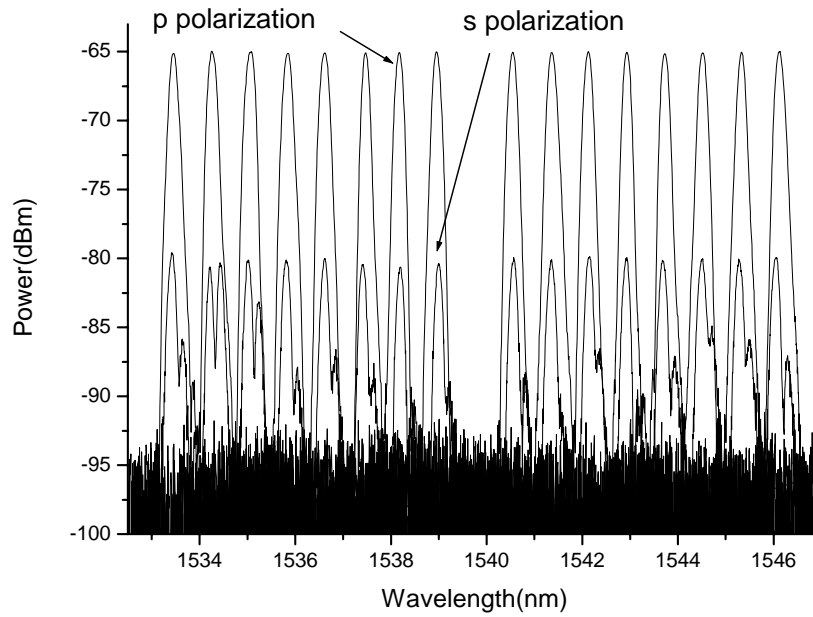


Fig. 3-16 Power-equalized output of the 16 channels of the LC-DEMUX

Table 3-1 The measure data for 16-channel LC-multi-DEMUX

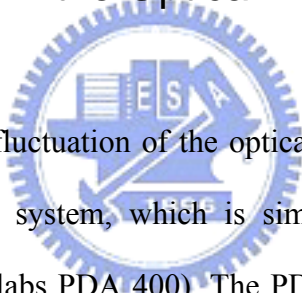
channel	ITU grid (nm)	Experiment (nm)	ITU-Experiment	Extinction ratio(dBm)	Power Equalizer 16channel	Ripple Level(dBm)
1	1533.468	1533.48	-0.012	14.216	-65.121	-0.121
2	1534.253	1534.21	0.043	12.445	-64.978	0.022
3	1535.038	1535.02	0.018	13.769	-64.99	0.01
4	1535.825	1535.83	-0.005	14.085	-65.116	-0.116
5	1536.612	1536.59	0.022	12.085	-65.086	-0.086
6	1537.4	1537.4	0	13.966	-65.067	-0.067
7	1538.189	1538.2	-0.011	11.491	-65.055	-0.055
8	1538.978	1538.98	-0.002	15.665	-65.008	-0.008
9	1540.56	1540.56	0	16.107	-65.027	-0.027
10	1541.352	1541.34	0.012	16.237	-65.045	-0.045
11	1542.145	1542.13	0.015	12.562	-64.997	0.003
12	1542.939	1542.93	0.009	13.387	-65.041	-0.041
13	1543.733	1543.73	0.003	13.688	-65.145	-0.145
14	1544.529	1544.52	0.009	13.1	-65.087	-0.087
15	1545.325	1545.28	0.045	11.119	-65.035	-0.035
16	1546.122	1546.08	0.042	12.565	-64.962	0.038
Average			0.01175	13.5304375	-65.0475	-0.0475
Max			0.045	16.237		
Min			0	11.119	Fluctuation	0.145+0.038=0.1925

Chap4

Optical Demultiplexer feedback control Pixel Equalizer

Variable optical attenuators (VOAs) play an importance role in regulating and dynamically equalizing channel powers in wavelength division multiplexed (WDM) networks. In chapter 3, we demonstrate a useful LC-multi-fiber VOA, LC-SLM. In this chapter, we hope to reduce ripple level and easy to control, then add this spectral component, Digital variable resistor for the feedback control by PC system.

4.1 Power fluctuation in the Optical Demultiplexer System



We measure the power fluctuation of the optical demultiplexer system without LC-SLM. Fig. 4-1 show the system, which is similar to Fig. 3-1 except single replacing photodetector (Thorlabs PDA 400). The PDA 400 is amplified photodiode in a compact package. A wide bandwidth (1000 nm ~ 1650 nm), low noise amplifier boosts the output of the high-speed PIN photodiodes for detection of low-level signals. Connectorized fibers can be easily attached to the PDA using one of the fiber adapters. The PDA400 adds near-infrared response and adjustable gain to the selection. A large 1mm diameter InGaAs photodiode provides ease of use. A 5-position rotary switch allows the gain to be increased from 1.5×10^4 V/A to 1.5×10^4 in precise 10dB increments for repeatable measurements. The PDA400 has a 10MHz bandwidth at the minimum gain setting.

Fig. 4-2 shows the power ripple level of the Demux system. Before 62500 sec, the temperature variation of the laboratory is about 1.8°C , the power fluctuation of the system is about 0.7V or 24%. If we just look for the temperature stable range, Fig. 4-2(b) shows the fluctuation is 2.4%. After 62500 sec, we open the old-type air conditioner, which produce the air perturbation motion to influence the system stable. Fig. 4-3(c) shows the fluctuation is 5.26%.

Form these experiment results; we understand that the Demux system needs the temperature and shock control or the feedback control to restrain the each kinds of fluctuation. In order to reduce power ripple level and easy to control, we choose the feedback control system.

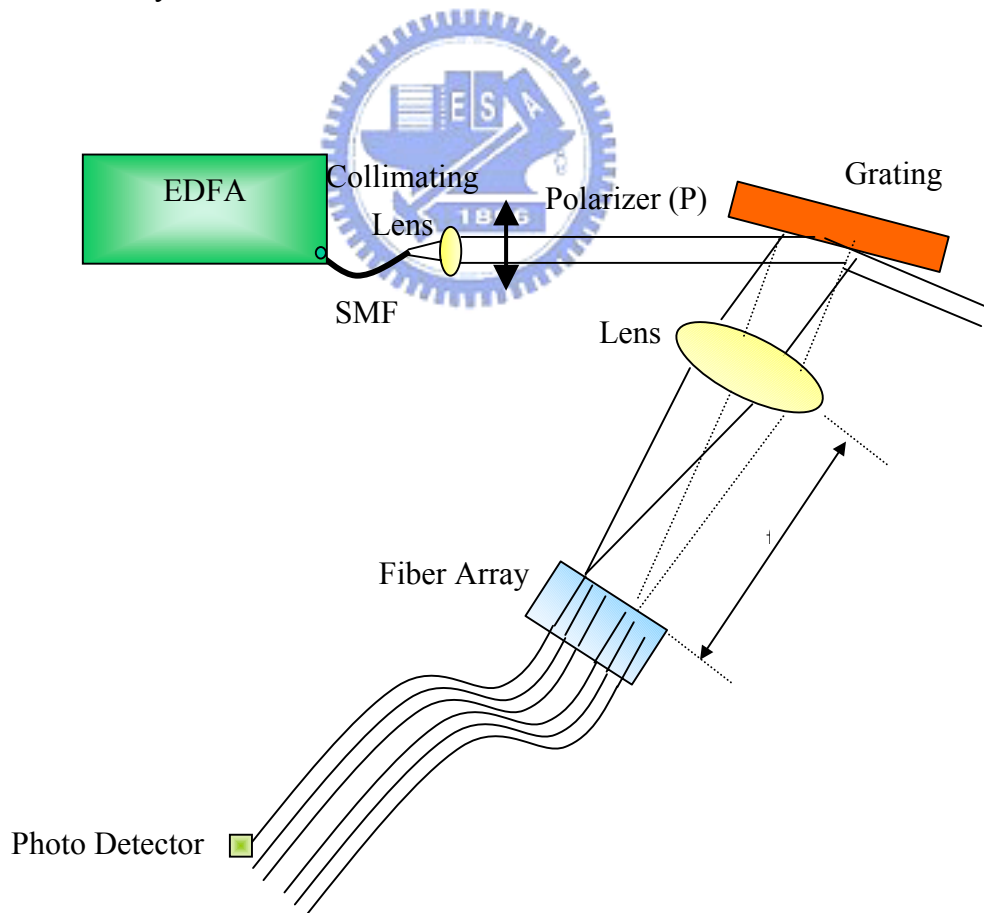
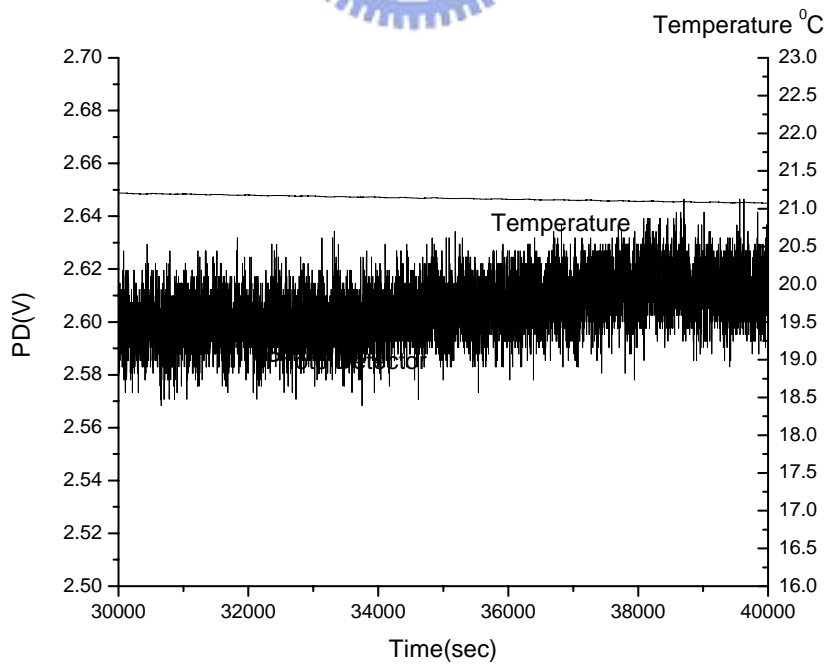
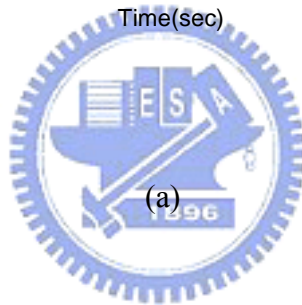
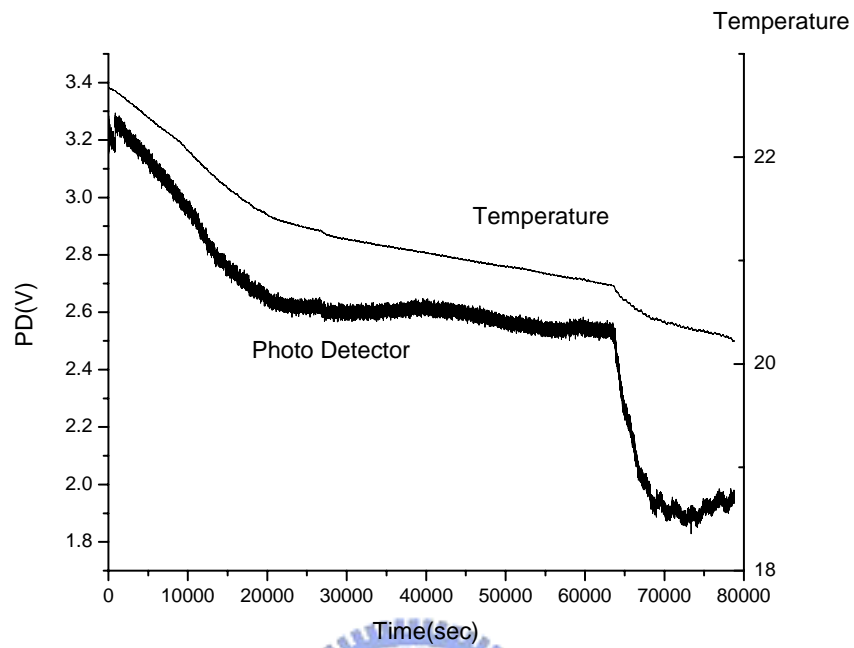


Fig. 4-1 Optical demultiplex of spectrum of P-state polarization and Photo detector.



(b)

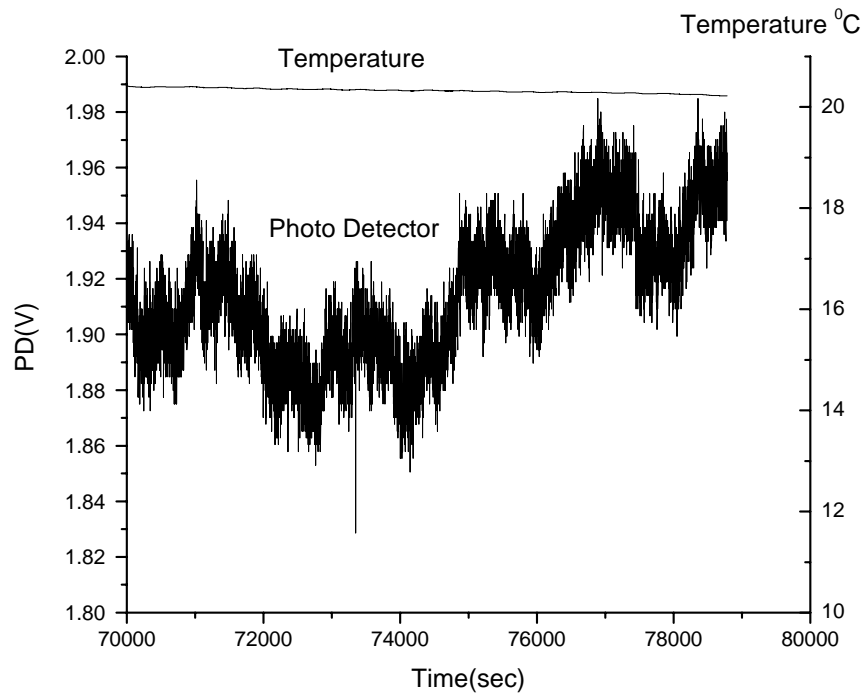
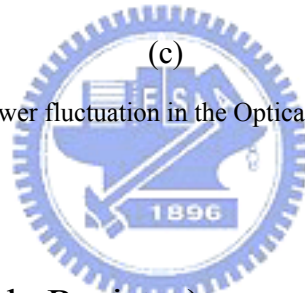


Fig. 4-2 (a)(b)(c) Power fluctuation in the Optical Demultiplexer System



4.2 Digital VR (Variable Resistor)

The Digital Variable Resistor, which is the variable resistor we can control resistance by the digital signal from PC or other kinds of digital function generator. From Sect. 2.2.3, we employ the VR resistance to modulate the voltage on the LC-SLM.

4.2.1 Feature of Digital VR GS6267

The Digital VR was bought by Link as (www.linkas.com.tw). Details of the information can be found in the web. A brief summary is given below.

- (1) Including 2 sets of 256 steps Digital VR, which are controlled by digital signal.
- (2) The total resistance is 10k ohm per each Digital VR, which can be used separately or cascade serially as 1 set only with total resistance is 20k ohm. (In this paper, Digital VR, which is parallel connection as 1 set with total resistance is 5k ohm of 512 steps.)
- (3) The resistance of Digital VR can be set, or read by 3-wire controlled methods.
(EN, Enable Control Input; CLK, Clock Control Input; Din, Data Input)

4.2.2 Operations of Digital VR GS6267

GS6267 included 2 sets of Digital VR, which are combined by 256 steps of small resistor elements. And its resistance is controlled by digital signal. The total resistance of each set of Digital VR is 10 k ohm, which can be used separately. The resolution of Digital VR GS6267 is 10k ohm / 256 steps, or 20k ohm / 512 steps (cascade serially), or 5k ohm / 512 steps (parallel connection). When power on, the initial value of each Digital VR's wiper position is set at 50% of total resistance, or binary code 1000 0000.

The resistance of Digital VR, is controlled by Enable Control Input (EN), Clock Control Input (CLK), and Data Control Input (Din), 3 signals.

CLK: The operation frequency range of signal of Clock Control Input (CLK) is from DC to 10 M Hz, Which offered the synchronous timing base for Data Control Input or Output.

Din: The signal of Data Control Input (Din) come into the device when Clock Control Input (CLK) signal transit from low voltage level to high voltage level.

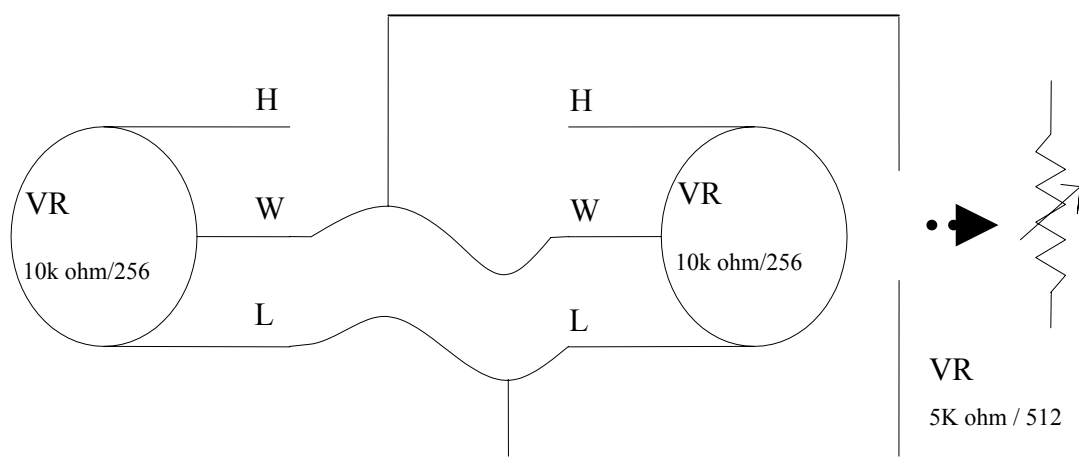
EN: The signal of Enable Control Input (EN) is a high active signal, i.e. EN must be in high voltage level when communicating between CLK, or Din with device.

When end of communication, the signal of Enable Control Input (EN) must return to low voltage level for preventing the noise through the Clock Control Input port (CLK) and Control Data Input Port (Din) to make an incorrect action.

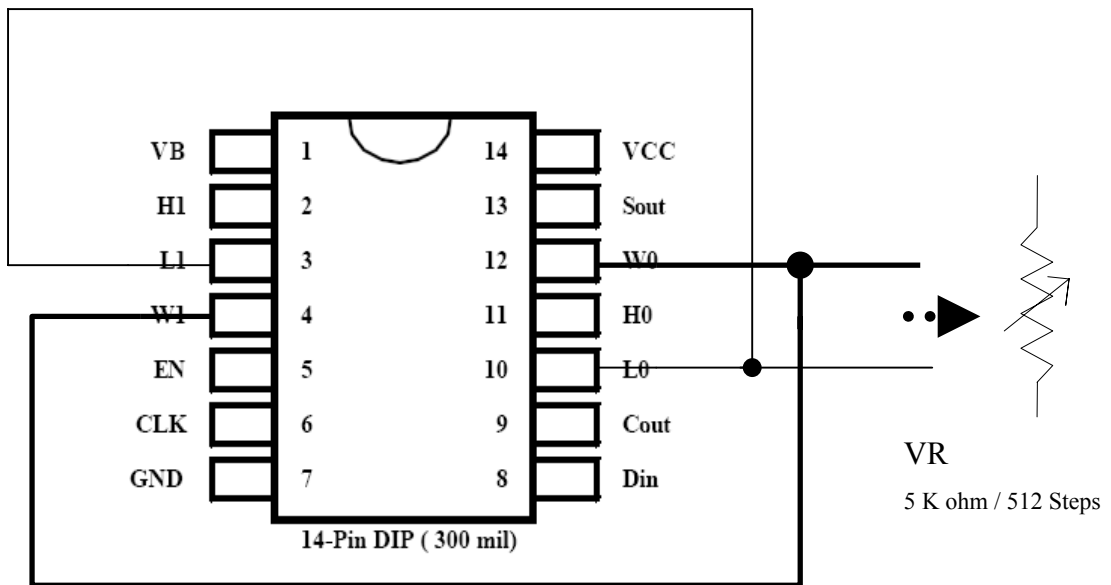
4.2.3 Structure of Digital VR

In this paper, Digital VR, which is parallel connection as 1 set with total resistance is 5k ohm of 512 steps. We will introduce the structure here.

The popular variable resistor, have H, W and L. H: High voltage End of VR. W: Output of VR. L: Low voltage end of VR. This structure is the same with Digital VR. When we parallel connection two VR, the resolution of Digital VR is 5k ohm / 512 steps. Fig 2.13 shows the sketch (a) and real device fig (b)(c).



(a)



(b)



(c)

Fig. 4-3 Structure of Digital VR (a) Sketch (b) real device structure fig (c) picture of real object

4.2.4 Basic theory of LC-SLM De-mux feedback control system

The LC-SLM driving circuit is shown in Fig.4-4. V_{sin} is the function generator; $5Kohm$ is the popular resistance; $VR1\sim4$ are the Digital Variable Resistances and $LC1\sim4$ are the pixels of LC-SLM. The digital variable resistor is used to change the voltage across the TN-SLM by varying the resistor value of variable resistor.

Fig. 4-5 shows the transmittance of the LC-SLM, we suppose that the transmittance-voltage linear range is 0~80% and 2~4Vrms. Then, we will got the transmittance equation:

$$V_{LC} = V_C * \frac{5Kohm}{5kohm + VR(0 \sim 5kohm, 0 \sim 512Steps)} \quad (4.1)$$

Where V_{LC} is the voltage across the LC-SLM, V_C is the voltage of function generation (Vrms), VR is the ohm of Digital Variable Resistance, and T is the transmittance of the LC-SLM.

When V_C is 4 Vrms and VR is 5, 0 and 2.5Kohm, the each transmittance of the LC-SLM is 0, 80 and 45 %. The equations are (4.2), (4.3) and (4.4):

$$V_C = 4Vrms; VR = 5kohm(512Step) \rightarrow V_{LC} = 2Vrms \rightarrow T \approx 0\% \quad (4.2)$$

$$V_C = 4Vrms; VR = 0kohm(0Step) \rightarrow V_{LC} = 4Vrms \rightarrow T \approx 80\% \quad (4.3)$$

$$V_C = 4Vrms; VR = 2.5kohm(256Step) \rightarrow V_{LC} = 2.67Vrms \rightarrow T \approx 45\% \quad (4.4)$$

In order to figure Eq. (4.1) out, we simulate equation for mathematica 3.0 shown in Fig. 4-6. Form Fig. 4-6(b) we get the useful theory if we can control the Digital VR steps, the transmittance of LC-SLM will be modulate control.

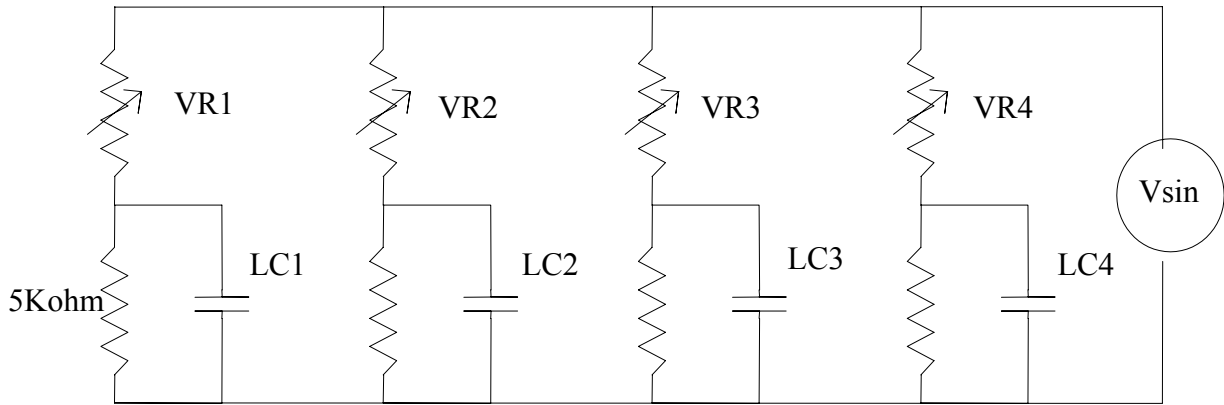


Fig. 4-4 The LC-SLM driving circuit for Digital variable resistor feedback control.

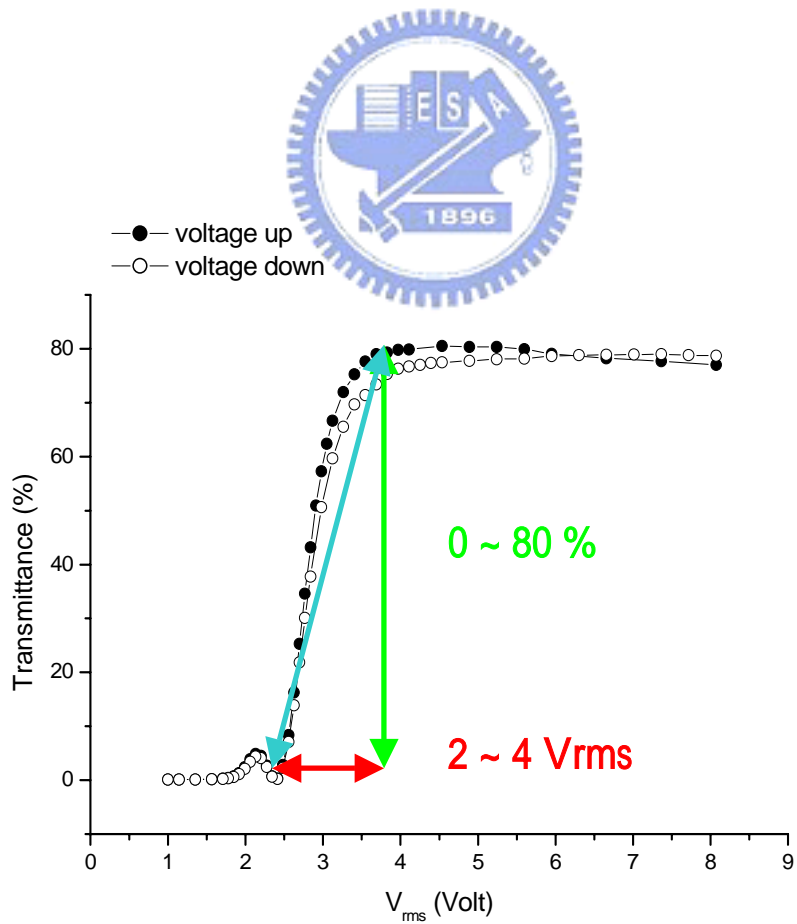
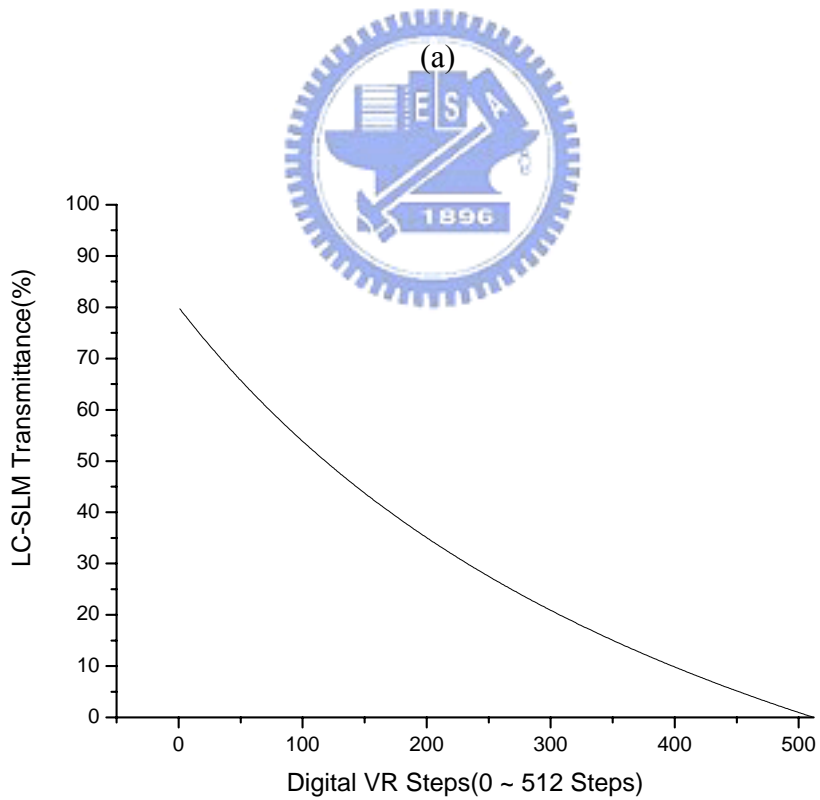
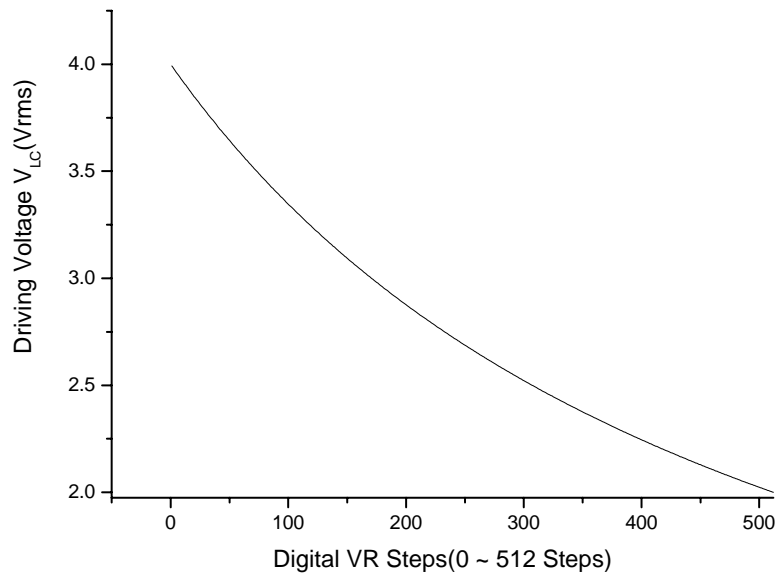


Fig. 4-5 The transmission curve of the LC-SLM by power meter and approximate linear range.



(b)

Fig. 4-6 Simulate Figure of Digital VR Steps to (a) LC-SLM pixel driving voltage and (b) LC-SLM pixel transmittance by Mathematica 3.0

4.3 Optical demultiplexer feedback control pixel equalizer experiment

Fig. 4-7 shows my last system, which add the Digital variable resistors feedback control device include photo detectors, 5k ohm popular resistances Digital VR, function generation, and PC. The PD1 connect with fiber array channel 3 of wavelength 1535.04 nm, PD2 with channel 7 of wavelength 1538.19 nm, PD3 with channel 10 of wavelength 1541.35 nm, and PD4 with channel 13 of wavelength 1543.73 nm.

When the spectrally dispersed beam focused on the fiber array, the designated photodetector receive the power intensity and then PC will compare the power intensity. If the intensity value is higher than the control add scope value, the digital VR is reduced one step and if the intensity value is lower than the control subtract scope value, the digital VR is raised one step.

Fig. 4-8 shows the experiment data results. We set the power equalizer control value is 3V and Power fluctuation is 0.93% (scope value = 0.014V).

According to $P_{\text{peak to peak}} / P_{\text{Control}}$, Fig. 4-8 (a)(b)(c)(d) represent that power fluctuation of optical demultiplexer feedback control pixel equalizer is 1.186 %, 2.17%, 3.84 % and 1.175% within about 9000 sec.

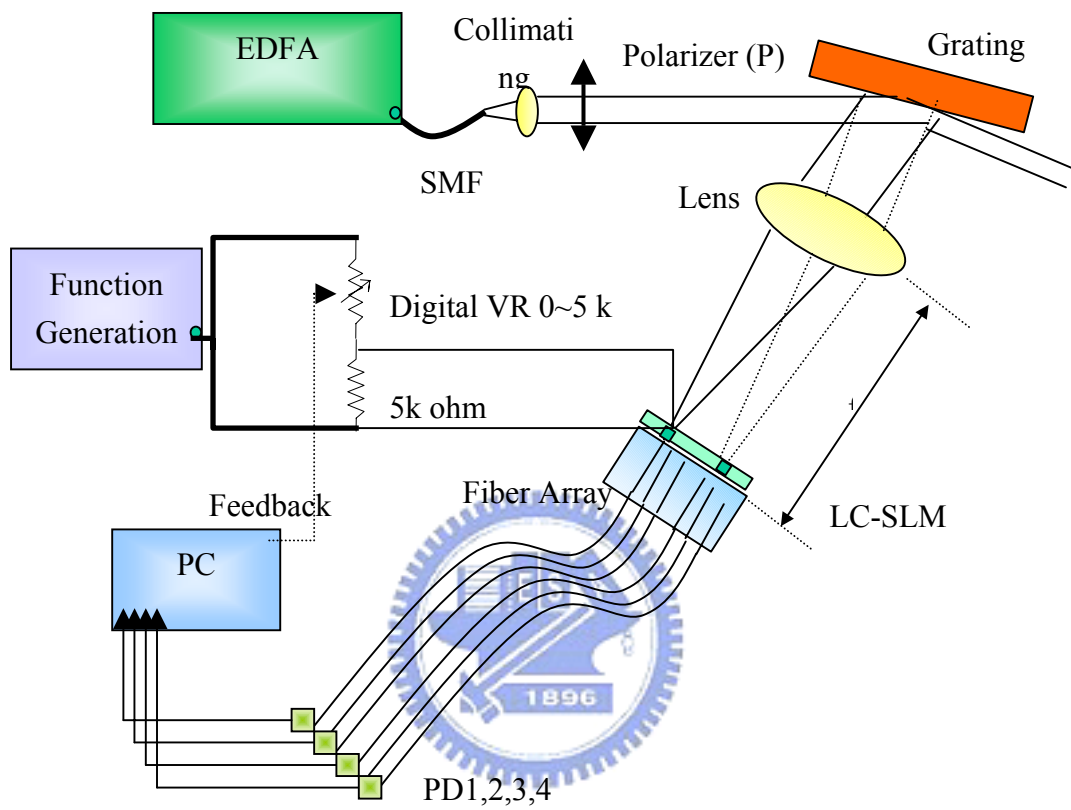
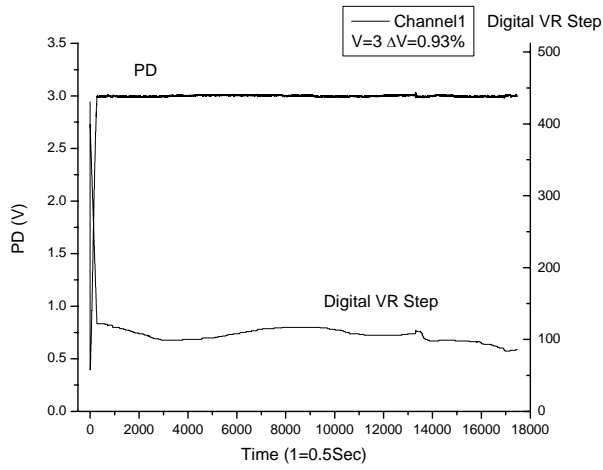
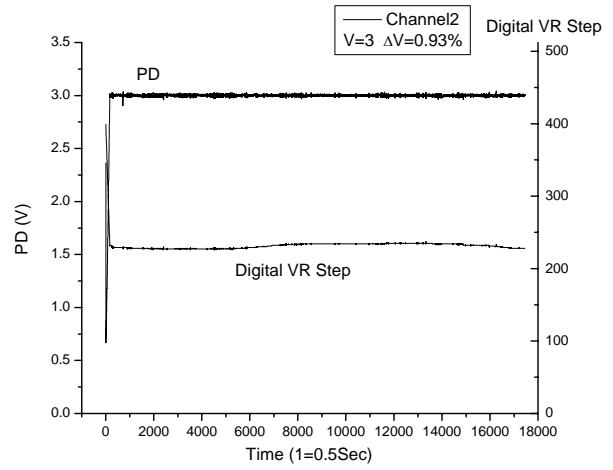


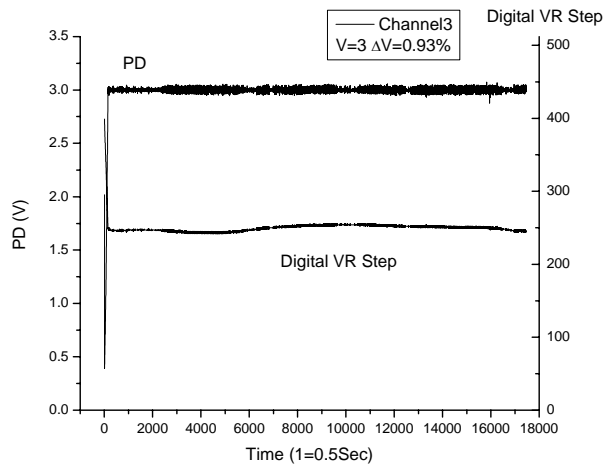
Fig. 4-7 Tunable Optical Demultiplexer feedback control Pixel Equalizer with LC-based



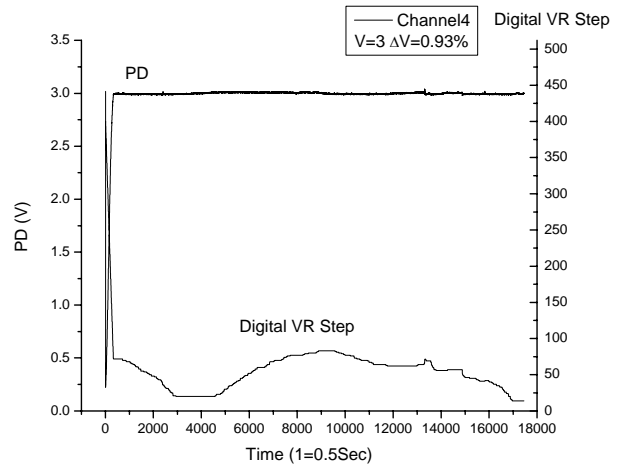
甲、



(b)



(c)



(d)

Fig. 4-8 Power stability of Optical Demultiplexer Pixel Equalizer with LC-based LC-SLM and Digital

VR by photo detector. PC control parameter is “Power equalizer control value is 3V and

Power fluctuation is 0.93 %”

(a) Channel1 Power Fluctuation = $0.0356/3 = 1.186\%$

(b) Channel2 Power Fluctuation = $0.0651/3 = 2.17\%$

(c) Channel3 Power Fluctuation = $0.11527/3 = 3.84\%$

(d) Channel4 Power Fluctuation = $0.03526/3 = 1.175\%$

We see that each channels power fluctuation is different. Fig. 4-9 will show the reason. From Fig. 4-9 the power level is modulated by the Digital VR step. But the adjusted value is not enough or mean the modulate slope is larger. Fig 4-9(a) channel 2 sometimes the power pass the control range because of large modulate slope and Fig 4-9(b) channel 3 always the power pass the control range, which will raise the perturbation and power fluctuation. This question can be solving easily by increasing the Digital VR steps, if we can get the one.

Fig. 4-10 shows another experiment data results. We change the control parameters of power equalizer control value is 2.5V and Power fluctuation is 0.9% (scope value = 0.01125V). According to $P_{\text{peak to peak}} / P_{\text{Control}}$, Fig. 4-10 (a)(b)(c)(d) represent that power fluctuation of optical demultiplexer feedback control pixel equalizer is 1.1 %, 3.48 %, 1.432 % and 1.368% within about 5000 sec.

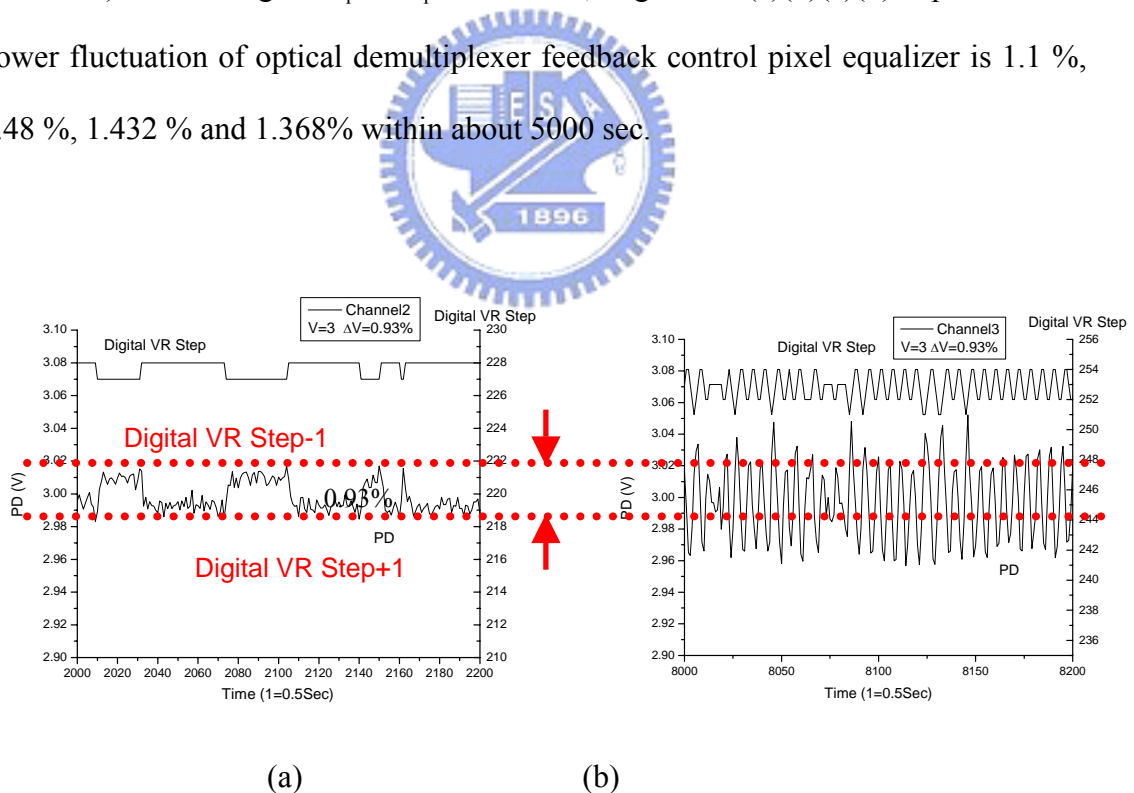


Fig. 4-9 Power stability of Optical Demultiplexer Pixel Equalizer with LC-based LC-SLM and Digital VR by photo detector.

(a) Channel2 (b) Chmmel3

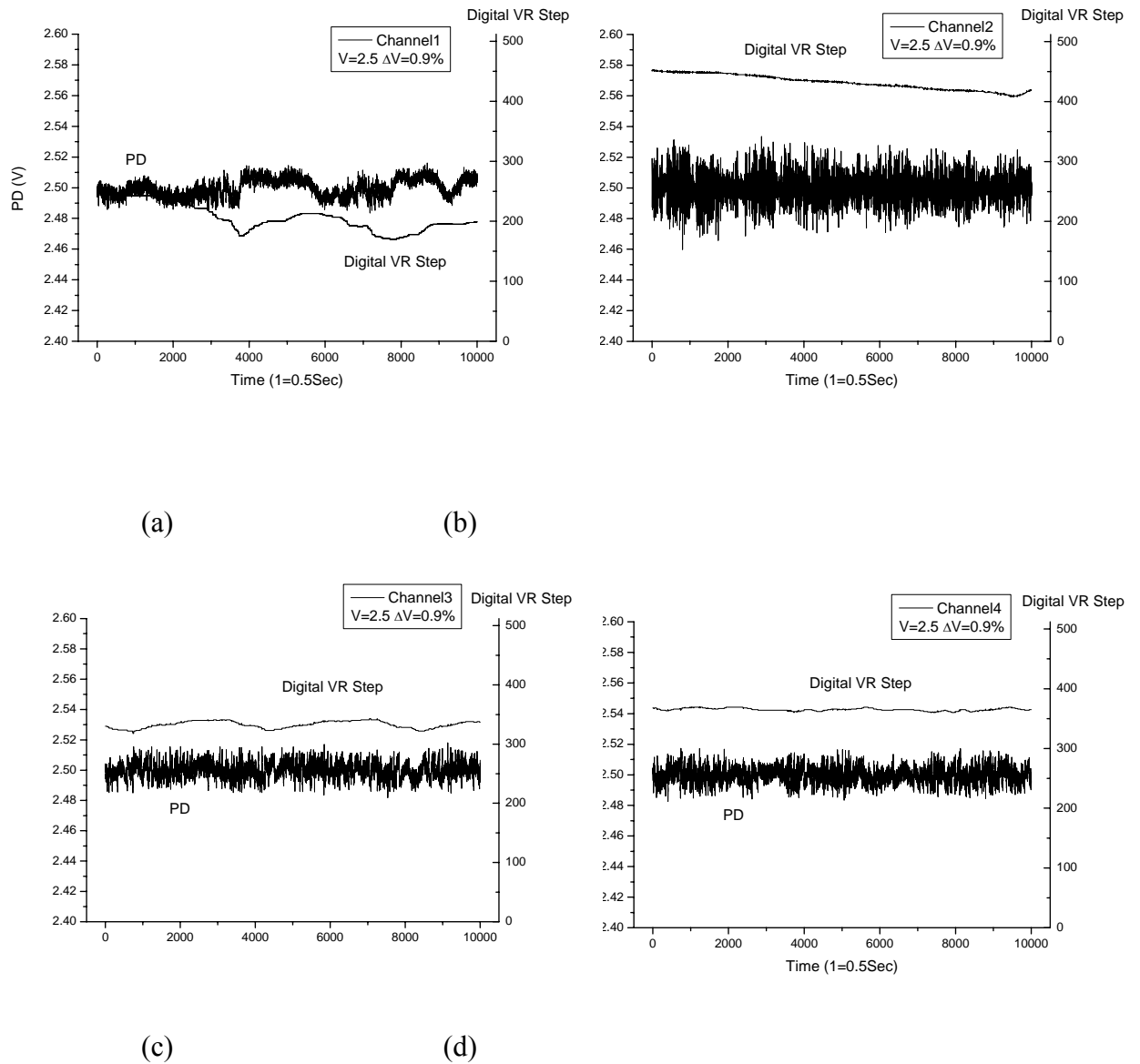


Fig. 4-10 Power stability of Optical Demultiplexer Pixel Equalizer with LC-based LC-SLM and

Digital VR by photo detector. PC control parameter is “Power equalizer control value is 2.5V and Power fluctuation is 0.9 %”

(a) Channel1 Power Fluctuation = $0.033/2.5 = 1.1\%$

(b) Channel2 Power Fluctuation = $0.087/2.5 = 3.48\%$

(c) Channel3 Power Fluctuation = $0.0358/2.5 = 1.432\%$

(d) Channel4 Power Fluctuation = $0.0342/2.5 = 1.368\%$

4.4 Optical demultiplexer feedback control pixel equalizer discussion

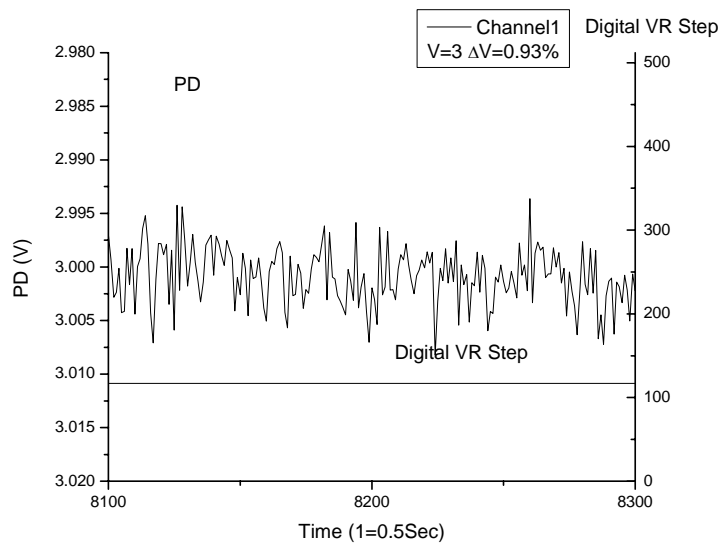
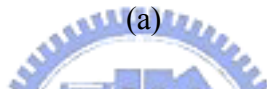
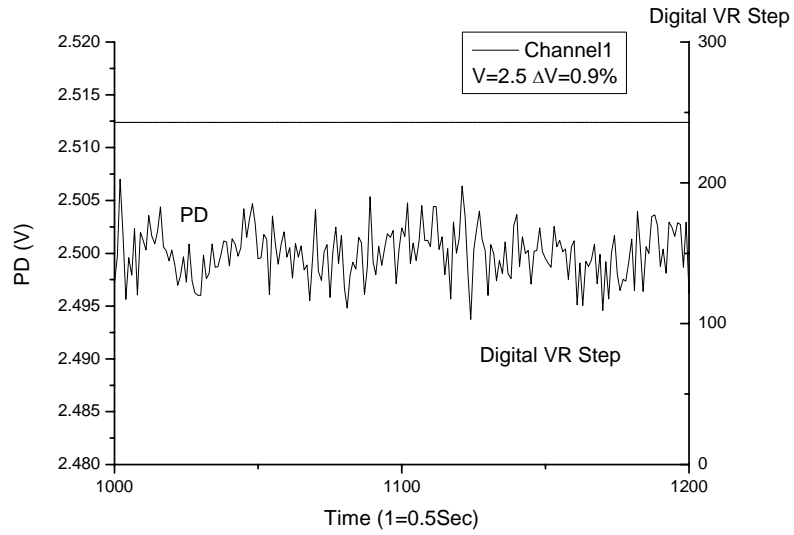
Here we discuss the experiment data. In chapter 3 we get 0.2dB fluctuation of 16-channel LC-multi-DEMUX, which change to percent is 4.6 %. The change equation of the symbol can be described as:

$$F = 0.2dB = 4.6\% \quad (10^{\frac{0.1}{10}} - 10^{\frac{-0.1}{10}} = 0.046) \quad (4.5)$$

In chapter 4 we get 1.2% fluctuation of Optical Demultiplexer feedback control Pixel Equalizer, which change to dB is 0.052 dB. The change equation of the symbol can be described as:

$$F = 1.2\% = 0.052dB \quad (10\log_{10} 1.006 - 10\log_{10} 0.994 = 0.052) \quad (4.6)$$

Our feedback control system reduced the system power fluctuation. We do not think 1.2% is the ultimate of our feedback control system. Fig. 4-11 shows the data within about 100 sec, the Digital VR step does not vary; the fluctuation of this data is 0.3% or 0.013dB. In other words, if we can increase the Digital VR steps, the fluctuation of system will be lower to about 0.3%. From our experiment data, 512 steps digital VR can produce the maximal fluctuation is 3.84 %, so we get the 0.3 % fluctuation, the steps would be 8192.



(b)

Fig. 4-11 Power stability of Optical Demultiplexer Pixel Equalizer with LC-based LC-SLM and

Digital VR by photo detector.

(a) $V=2.5$ $V=0.9\%$ Fluctuation=0.3% (b) $V=3$ $V=0.93\%$ Fluctuation=0.29%

4.5 Discussion and Summary

Finally we studied some latest papers of LC-VOA and other kinds of VOA feedback control system. Let us to discuss these components advantage and characteristics.

1. LC-based VOA on fiber arrays [47]

We have developed simple and inexpensive level equalizer arrays using 8- to 16-channel independent liquid-crystal (LC) variable-optical-attenuator (VOA) arrays and multichannel in-line photodetector arrays, which were integrated on fiber arrays. We used two types of LC-VOAs: (1) ultrathin LC cells inserted into trenches cut across the fiber arrays, and (2) LC filling the gap between transparent electrode-coated fibers of the fiber splicer. The pitch of the fibers was 250 μm , and the number of fibers ranged from 8 to 16. These level equalizer arrays can suppress 2-Hz power fluctuations to a desired constant power level by using a dithering feedback circuit. First type the attenuation range is 8.2 to 11.2 dB, the polarization dependence is 3.1 to 5.6 dB, the voltage is 16.7 to 26.4 Vrms; second type the attenuation range is 18 to 26.2 dB, the polarization dependence is 8.3 to 21 dB. The voltage is 2.7 to 6.9 Vrms. These level equalizer arrays made it possible to keep fluctuations of the input light power at an almost constant level (40 W) with the fluctuation of about 0.5 dB which was due to the dithering.

2. Cutoff modulator with tapered waveguides VOA [48]

A variable optical attenuator was demonstrated by using a thermo-optic cutoff modulator in polymers. It combined horizontally and vertically tapered waveguide structures to improve both the attenuation efficiency and the fiber coupling. The

measured insertion loss of the attenuator was 2.5 dB at 1550 nm. The dynamic range was more than 20 dB with an electrical power consumption of 160 mW. And the optical response time was faster than 1.5 ms. The effect of polarization on the attenuation was reduced to 0.1 dB by employing a continuous electronic feedback control. The wavelength uniformity was as small as 0.3 dB over the range from 1530 to 1560 nm.

3. Polymeric feedback control VOA in WDM systems [49]

A variable optical attenuator is described which uses an asymmetric polymeric Y-branch waveguide. It incorporates an optical monitoring tap to regulate the optical output regardless of attenuation range was >18dB. The attenuator was used to regulate channel powers within 0.5dB in WDM system.

4. Fault tolerant VOA using three dimensional beam spoiling [50]

A variable fiber-optic attenuator (VFOA) in a compact folded optical structure is introduced using the basic principles of optical beam misalignment via three-dimensional (3-D) beam spoiling. Key features include high resolution of control, the ability to tune the attenuation response, and the fault tolerant attenuator design. Experimental proof of concept demonstration using one dual fiber collimator and a three-axis controlled mirror as a 3-D beam spoiling element shows a high 52.4 dB dynamic range and a very low optical loss of 0.12 dB at 1550 nm wavelength. The measured polarization dependent loss is 0.02 dB. In addition, multi-wavelength VFOA performance indicates an average 52.4 dB maximum optical attenuation with a ± 0.04 dB fluctuation over a 70 nm bandwidth. A wavelength dependent loss of 0.10 dB is also measured with a fluctuation of ± 0.04 dB. **Table 4-1** summarizes the data of the variety VOA and our Demultiplexer feedback control pixel equalizer.

Table 4-1 The data of the Variety VOA

	Ripple level (dB)	Wavelength (nm)	Insertion loss(dB)	Attenuation (dB)	PDL (dB)
Demultiplexer feedback control pixel equalizer	0.052dB	1533 ~ 1547	1 ~ 3dB (LC-SLM)	11.1 ~ 16.2dB	
LC-based VOA on fiber arrays	0.5dB		0.7dB (fiber to fiber loss)	(1) 8.2 ~ 11.2 (2) 18 ~ 26.2	(1)3.1~5.6 (2)8.3~21
Cutoff modulator with tapered waveguides VOA	0.3dB	1530 ~ 1560	2.5dB	20dB	
Polymeric feedback control VOA in WDM systems	0.5dB			>18dB	<0.6dB
Fault tolerant VOA using three dimensional beam spoiling	± 0.04dB		0.12dB	52.4dB	0.02dB

Chapter 5

Conclusions

5.1 Conclusions

In this thesis, we have designed and demonstrated a liquid-crystal-based 16-channel DEMUX with 100-GHz channel spacing and Optical Demultiplexer feedback control Pixel Equalizer. It consists of EDFA, a collimating lens, grazing-incident grating, image lens, a transmission-type liquid crystal spatial light modulator (LC-SLM), fiber array for output, OSA, photodetector, and digital variable resistor, and computer. In this system, first-order diffracted signal light by the grating is directed to the image lens and focused on to the LC-SLM and fiber array. Selecting the appropriate LC-SLM pixels allows light of the desired wavelength to transmit into the fiber array.

In chapter 3, the center wavelengths of the channels are designed and the channels are designed according to the International Telecommunication Union (ITU) grid with channel spacing of 100 GHz. The crosstalk between channels is less than -30 dB. The average 1 dB and 3 dB passbands of the DEMUX are 12.5 and 22.5 GHz, respectively. The center wavelength of each channel is accurate to 0.04 nm. The extinction ratios for pixels on/off for the 16 channels range from 11.1 dB to 16.2 dB. The average extinction ratio is 13.53 dB. This approach enables additional functionalities of the DEMUX, such as dynamic gain equalization. The outputs of the channels of the LC-multi-DEMUX are equalized to -65 dBm and the variation between different channels are reduced from ~ 10 dB to less than 0.5 dB.

In chapter 4, we have demonstrated optical demultiplexer feedback control pixel equalizer to reduce ripple level and easy to control of LC-multi-DEMUX. We selected four channels to feedback control the power level, the fluctuation is reduced to 1.2% or 0.052dB. We can modulate the transmittance of LC-SLM to adapt to the different conditions and change the each channel power easily independently by PC.

5.2 Future works

1. We expect to reduce channel spacing from 100 GHz to 50 GHz, even 25 GHz by selecting the appropriate focal length of lens and groove spacing or diffraction order of the grating.
2. We can balance the insertion loss by adding another EDFA on output fibers.
3. There are not the real output in our system, we select the applicable fiber coupler to add the real output.
4. Our system is Polarization sensitivity. There is large Polarization dependence loss. We can change the Polarization-independent grating.
5. We need to increase the Digital VR steps to raise the power stabilization. If we can get 8192 or more steps Digital VR, we think the power fluctuation will be 0.3 %.

Reference

- [1] F. Zhao, J. Qiao, R. Chen et al., "Reliable grating-based wavelength division (de)multiplexers for optical networks," *Opt. Eng.*, vol. 40, pp. 1204-1211, 2001.
- [2] K. Sano, R. Watanabe, and J. Minowa, "A 4-wavelength optical multi/demultiplexer for WDM subscriber loop systems using analog baseband video transmission," *IEEE Journal of Lightwave Technology*, pp. 631-639, 1986.
- [3] R. H. Qu, H. Zhao, Z. J. Fang, E. Marin, and J. P. Meunier, "Configurable wavelength-selective switch based on fiber grating and fiber loop mirror," *IEEE Photon. Technol. Lett.*, vol. 12, pp. 1343-1345, 2000.
- [4] K. Takada, M. Abe, M. Shibata, M. Ishii, and K. Okamoto, "Low-crosstalk 10-GHz-spaced 512-channel array-waveguide grating multi/demultiplexer fabricated on a 4-in wafer," *ibid.*, vol. 13, pp. 1182-1184, 2001.
- [5] G. R. Hill, "Wavelength domain optical network techniques," *Proc. IEEE.*, vol. 78, pp. 121-132, 1990.
- [6] M. J. O'Mahoney, "Optical multiplexing in fiber networks: Progress in WDM and OTDM," *IEEE Commun. Mag.*, vol. 33, pp. 88-, 1995.
- [7] G. E. Keiser, "A review of WDM technology and applications," *Optical Fiber Technology*, vol. 5, pp. 3-39, 1999.
- [8] R. E. Wagner, R. C. Alfferness et al., "MONET: Multiwavelength optical networking," *IEEE Photon. Technol. Lett.*, vol. 14, pp. 1349-1355, 1996.
- [9] V. Mizrahi, S. Alexander, J. Berthold, S. Chaddick, and W. Jones, "The future of WDM system," *ECOC'97*, no. 448, pp. 137-141, Sept. 1997.

- [10] J. W. Ready and J. R. Jones, "Methods of collision detection in fiber optic CSMA/CD networks," *IEEE J. on Selected Areas in Commun.*, vol. SAC-3, no.6, pp. 890-896,1985.
- [11] C. R. Doerr, C. H. Joyner, and L. W. Stulz, "Integrated WDM Dynamic Power Equalizer with Potentially Low Insertion Loss", *IEEE Photonics Technology Letters*, vol. 10, No. 10, October 1998.
- [12] C. R. Doerr, M. Cappuzzo, E. Laskowski, A. Paunescu, L. Gomez, L. W. Stulz, and J. Gates, "Dynamic Wavelength Equalizer in Silica Using the Single-Filtered-Arm Interferometer", *IEEE Photonics Technology Letters*, Vol. 11, No. 5, May 1999.
- [13] B. J. Offrein, F. Horst, G. L. Bona, R. Germann, H. W. M. Salemink, and R. Beyeler, "Adaptive Gain Equalizer in High-Index-Contrast SiON Technology", *IEEE Photonics Technology Letters*, Vol. 12, No. 5, May 2000.
- [14] K. Suzuki, T. Kitoh, S. Suzuki, "PLC-based dynamic gain equalizer consisting of integrated Mach-Zehnder interferometers with C- and L-band equalising range", *Electronics letters* 29th August 2002 Vol.38 No.18.
- [15] Z. G. Lu, P. Lin, and C. P. Grover, "A dynamically gain-flattened erbium-doped fiber amplifier", *Microwave and Optical Technology Letters*, Vol. 39, No. 1, October 5 2003.
- [16] Seok Hyun Yun, Bong Wan Lee, Hyang Kyun Kim, and Byoung Yoon Kim, "Dynamic erbium-doped fiber amplifier based on active gain flattening with fiber acoustooptic tunable filters", *IEEE Photonics Technology Letters*, Vol. 11, No. 10, October 1999.
- [17] Ashish M. Vengsarkar, J. Renee Pedrazzani, Justin B. Judkins, and Paul J. Lemaire, "Long-period fiber-grating-based gain equalizers", *Optics Letters*, Vol. 21, No. 5, March 1, 1996.

- [18] In Kag Hwang, Seok Hyun Yun, and Byoung Yoon Kim, “Long-period fiber gratings based on periodic microbends”, *Optics Letters*, Vol. 24, No. 18, September 15, 1999.
- [19] Ik-Bu Sohn, Nam-Kwon Lee, Hyung-Woo Kwon, Jae-Won Song, “Tunable gain-flattening filter using microbending long-period fiber gratings”, *Opt. Eng.* 41(7) 1465–1466 (July 2002).
- [20] Kazuyou Mizuno, Yu Mimura, Osamu Aso, Shu Namiki and An Yo, “Application of Nonlinear Fitting for Etalon-Type Gain-Flattening Filter Design”, *Jpn. J. Appl. Phys.* Vol. 42 (2003) pp. 456 – 460.
- [21] Tizhi Huang, Jeff Huang, Yueai Liu, Ming Xu, Yatao Yang, Minchun Li, “Performance of a Liquid-Crystal Optical Harmonic Equalizer”, OFC2001, Optical Fiber Communication Conference, Postdeadline paper, March 2001.
- [22] Jung-Chih Chiao and Tizhi Huang chorum Technologies, “Liquid-Crystal Optical Harmonic Equalizers”, The 27th European Conference on optical Communication(ECOC), Sept.30-Oct.4, 2001, Amsterdam, Netherlands.
- [23] Chongchang Mao, Ming Xu, Wei Feng, Jianyu Liu, and Jung-Chih Chiao, “Liquid-crystal Optical Switches and Signal Processors”, 2001 Asia-Pacific Optical and Wireless Communications Conference, Beijing, China, November 2001.
- [24] Katsuhiko Hirabayashi, Masato Wada, and Chikara Amano, “Optical-Fiber Variable-Attenuator Arrays Using Polymer-Network Liquid Crystal”, *IEEE Photonics Technology Letters*, Vol. 13, No. 5, May 2001.
- [25] Katsuhiko Hirabayashi, Masato Wada, and Chikara Amano, “Liquid Crystal Variable Optical Attenuators Integrated on Planar Lightwave Circuits”, *IEEE Photonics Technology Letters*, Vol. 13, No. 6, June 2001.

- [26] C. R. Doerr, L. W. Stulz, R. Pafchek, L. Gomez, M. Cappuzzo, A. Paunescu, E. Laskowski, L. Buhl, H. K. Kim, and S. Chandrasekhar, "An Automatic 40-Wavelength Channelized Equalizer", *IEEE Photonics Technology Letters*, Vol. 12, No. 9, September 2000.
- [27] C. R. Doerr, K. W. Chang, L. W. Stulz, R. Pafchek, Q. Guo, L. Buhl, L. Gomez, M. Cappuzzo, and G. Bogert, "Arrayed Waveguide Dynamic Gain Equalization Filter with Reduced Insertion Loss and Increased Dynamic Range", *IEEE Photon. Technol. Lett.*, Vol. 13, No. 4, April 2001.
- [28] N. A. Olsson and J. P. Van der Ziel, "Performance characteristics of 1.5- μ m external semiconductor lasers for coherent optical communication," *J. Lightwave Technol.*, vol. LT-5, pp. 510-515, 1987.
- [29] P. Zorabedian, "Axial mode instability in tunable external-cavity semiconductor lasers," *IEEE J. Quantum. Electron.* Vol. 30, pp. 1542-1552, 1994.
- [30] N. Kikuchi, Y. Liu, and J. Ohtsubo, "Chaos control and noise suppression in external-cavity semiconductor lasers," *IEEE J. Quantum. Electron.* Vol. 33, pp. 56-65, 1997.
- [31] J. R. Andrews, "Low voltage wavelength tuning of an external cavity diode laser using a nematic liquid crystal-containing birefringent filter," *IEEE Photonics Technol. Lett.*, vol. 2, pp. 334-336, 1990.
- [32] Maeda. M.W, Patel. J.S, Smith. D.A, Lin. C, Saifi. M.A, Lehman. A.V, "An electronically tunable fiber laser with a liquid-crystal etalon filter as the wavelength-tuning element," *IEEE Photonics Technol. Lett.*, vol. 2, pp. 787-789, 1990.
- [33] P. Mollier, V. Armbruster, H. Porte, and J. P. Goedgebuer, "Electronically tunable Nd-doped fibre laser using nematic liquid crystals," *Electron. Lett.*, vol. 31, pp. 1248-1250, 1995.

- [34] M. C. Parker, and R. J. Mears, "Digitally wavelength filter and laser," *IEEE Photonics Technol. Lett.*, vol. 8, pp. 1007-1008, 1996.
- [35] S. Matsumoto, M. Hirabayashi, S. Sakata, and T. Hayashi, "Tunable wavelength filter using nano-sized droplets of liquid crystal," *IEEE Photonics Technol. Lett.*, vol. 11, pp. 442-444, 1999.
- [36] K. Hirabayashi and T. Kurokawa, "Tunable wavelength-selective demultiplexer using a liquid-crystal filter," *IEEE Photonics Technol. Lett.*, vol. 4, no. 7, pp. 737-740, July 1992.
- [37] J. S. Patel and Y. Silberberg, "Liquid crystal and grating-based multiple-wavelength cross-connect switch," *IEEE Photonics Technol. Lett.*, vol. 7, no. 5, pp. 514-516, May 1995.
- [38] A. D. Cohen, M. C. Parker, and R. J. Mears, "100-GHz-Resolution dynamic holographic channel management for WDM," *IEEE Photonics Technol. Lett.*, vol. 11, no. 7, pp. 851-853, July 1999.
- [39] Jie Qiao, Feng Zhao, Ray T. Chen, James W. Horwitz, and William W. Morey, "Athermalized low-loss echelle-grating-based multimode dense wavelength division demultiplexer," *Appl. Opt.*, vol. 41, no. 31, pp. 6567-6575, 2002.
- [40] R.-P. Pan, X.-X. Tung, J.-Y. Chen, M.-J. Huang, and C.-L. Pan, "Liquid-crystal-based tunable optical filtering devices for DWDM," in *Proc. SPIE, Active and Passive Optical Components for WDM Communication*, vol. 4532, pp. 244-248, 2001.
- [41] C.-L. Pan, S.-H. Tsai, R.-P. Pan, C.-R. Sheu, and S. C. Wang, "Tunable semiconductor laser with liquid crystal pixel mirror in grating-loaded external cavity," *Electron. Lett.*, vol. 35, pp. 1472-1473, 1999.
- [42] R.-P. Pan, H.-C. Tung, C.-R. Sheu, M.-J. Huang and C.-L. Pan, "Wavelength Tunable Semiconductor Laser with a Liquid Crystal Pixel Mirror," in *Proc.*

- SPIE, Liquid Crystal Materials, Devices VIII Applications*, vol. 4658, pp. 91-100, 2002.
- [43] Robert P, F. Roeske, Jr. and D. E. Smith, “Fiber-optic spectral-steak equalizer”, *Rev. Sci. Instrum.*, vol. 56, pp. 1356-1362, 1985.
- [44] Garland Best et al, “Shedding light on hybrid optics: A tutorial in coupling,” *Optics & Photonics News.*, pp. 30-34, Feb., 1999.
- [45] Pochi Yeh and Claire Gu, *Optics of Liquid Crystal Display*, Wiley, 1999.
- [46] Chrong-Hann Niou, *Electronically tunable multi-wavelength active mode-locked semiconductor laser with a liquid crystal pixel mirror*, Master Thesis, IEO of NCTU Taiwan, 2001.
- [47] Katsuhiko Hirabayashi and Chikara Amano, “Liquid-Crystal Level Equalizer Arrays on Fiber Arrays”, *IEEE Photonics Technology Letters*, vol.16, no 2, February 2004.
- [48] Sang Shin Lee, Yong Sung Jin and Yung Sung Son, “Variable Optical Attenuator Based on a Cutoff Modulator with Tapered Waveguides in Polymers”, *Journal of Lightwave Technology*, vol. 17, no.12, December 1999.
- [49] Yong Sung Jin, Sang Shin Lee and Yung Sung Son, “Feedback Controlled Variable Optical Attenuator for Channel Power Regulation in WDM Systems”, *Electronics Letters*, vol.35, no.11, May 1999.
- [50] Nabeel A. Riza and Sarun Sumriddetchkajorn, “Fault-tolerant Variable Fiber-Optic Attenuator Using Three-Dimensional Beam Spoiling”, *Optics Communications*, pp. 103-108, November 2000.